RESEARCH ARTICLE

Ectopic assembly of an auxin efflux control machinery shifts developmental trajectories

Ana Cecilia Aliaga Fandino[1], Adriana Jelinkova[2], Petra Marhava[1], Jan Petrasek[2] & Christian S. Hardtke[1*]

[1] Department of Plant Molecular Biology, University of Lausanne, CH-1015 Lausanne, Switzerland

[2] Institute of Experimental Botany, Czech Academy of Sciences, 165 02 Prague, Czech Republic

Short title: Auxin efflux shift of xylem development

[*]Corresponding author: christian.hardtke@unil.ch

The author responsible for distribution of materials integral to the findings presented in this article in accordance with the policy described in the Instructions for Authors (https://academic.oup.com/plcell/pages/General-Instructions) is: Christian S. Hardtke (christian.hardtke@unil.ch).

Abstract

Polar auxin transport in the Arabidopsis (*Arabidopsis thaliana*) root tip maintains high auxin levels around the stem cell niche that gradually decrease in dividing cells but increase again once they transition towards differentiation. Protophloem differentiates earlier than other proximal tissues and employs a unique auxin 'canalization' machinery that is thought to balance auxin efflux with retention. It consists of a proposed activator of PIN-FORMED (PIN) auxin efflux carriers, the AGC kinase PROTEIN KINASE ASSOCIATED WITH BRX (PAX); its inhibitor, BREVIS RADIX (BRX); and PHOSPHATIDYLINOSITOL-4-PHOSPHATE-5-KINASE (PIP5K) enzymes, which promote polar PAX and BRX localization. Because of dynamic PAX-BRX-PIP5K interplay, the net cellular output of this machinery remains unclear. Here we deciphered the dosage-sensitive regulatory interactions between PAX, BRX and PIP5K by their ectopic expression in developing xylem vessels. The data suggest that the dominant collective output of the PAX-BRX-PIP5K module is a localized reduction in PIN abundance. This requires PAX-stimulated clathrin-mediated PIN endocytosis by site-specific phosphorylation, which distinguishes PAX from other AGC kinases. Ectopic assembly of the PAX-BRX-PIP5K module is sufficient to cause cellular auxin retention and affects root growth vigor by accelerating the trajectory of xylem vessel development. Our data thus provide direct evidence that local manipulation of auxin efflux alters the timing of cellular differentiation in the root.

Keywords: *Arabidopsis*, *auxin, AGC kinase, xylem, differentiation*

Introduction

The phytohormone auxin regulates plant development as well as adaptive responses by modulating growth patterns. Auxin action depends both on context and concentration, and is determined by an interplay of auxin biosynthesis, transport and signaling (Adamowski and Friml, 2015; Lavy and Estelle, 2016; Zhao, 2018). Long distance transport occurs in bulk through the plant vascular system, whereas short distance, cell-to-cell transport depends on dedicated plasma-membrane-integral auxin carriers (Morris and Kadir, 1972; Teale et al., 2006; Adamowski and Friml, 2015). They comprise the auxin influx facilitator AUX1 and its homologs, and the PIN-FORMED (PIN) auxin efflux carriers. The latter are chiefly responsible for creating the high local auxin concentrations that are observed in the growth apices of plants, the meristems (Blilou et al., 2005). Auxin maxima are associated with the formation of new, lateral organs, but are also required to maintain the meristems themselves. For example, the auxin maximum at the tip of Arabidopsis (*Arabidopsis thaliana*) root meristems is essential for the establishment and maintenance of the stem cell niche (SCN) (Sabatini et al., 1999). It is created by coordinated, generally rootward polar subcellular localization of PIN proteins in the stele and ground tissue, and reinforced by an "inverse fountain" of auxin recycling mediated by shootward-pointing PINs in the columella and epidermis (Grieneisen et al., 2007). The auxin maximum thus is the peak of an auxin gradient that determines the activity of transcriptional regulators, which in turn specify the different tissue layers and time their proliferation and differentiation (Mahonen et al., 2014).

PIN protein localization is a dynamic process that involves endocytic recycling and associated regulatory mechanisms. For example, phosphorylation of the cytoplasmic hydrophilic loop by the AGC kinase PINOID (PID) can induce PIN re-localization (Friml et al., 2004; Weller et al., 2017; Wang et al., 2023). Other AGC family kinases such as D6 PROTEIN KINASE (D6PK) also target phosphosites in the hydrophilic loop of PINs but thereby activate PIN-mediated auxin efflux from the cytoplasm into the apoplast (Willige et al., 2013; Barbosa et al., 2014; Zourelidou et al., 2014). PIN localization also depends on the low abundant plasma membrane phosphoinositide phosphatidylinositol-4,5-bisphosphate [PI(4,5)P2], which affects clathrin-mediated PIN endocytosis (Ischebeck et al., 2013; Tejos et al., 2014). PI(4,5)P2 is produced from the more abundant phosphatidylinositol-4-phosphate (PI4P) by PHOSPHATIDYLINOSITOL-4-

PHOSPHATE-5-KINASE (PIP5K) enzymes, like the redundant PIP5K1 and PIP5K2 in the Arabidopsis root.

The early vascular tissues of the root meristem, the protophloem and protoxylem, are formed inside the stele in a diarch pattern in Arabidopsis, wherein two protophloem poles are flanking an axis of metaxylem vessels that is delimited by protoxylem cell files on both sides (Supplemental Fig. S1). Molecular markers highlight both developing xylem vessels and protophloem sieve elements (the conducting cells of the protophloem) as sites of auxin response (Bishopp et al., 2011; Marhava et al., 2018), which is thought to promote their differentiation (Bishopp et al., 2011; Vaughan-Hirsch et al., 2018; Moret et al., 2020; von der Mark et al., 2022; Wang et al., 2023). For example, in *pip5k1 pip5k2* double mutants, frequent differentiation failures of xylem vessel precursors are associated with low auxin levels and can be partially rescued by induction of local auxin production (von der Mark et al., 2022). PIP5K1/2 are predominantly found in association with the plasma membrane but are also present in the nucleus (Gerth et al., 2017; Watari et al., 2022), and both subcellular localizations are required for normal xylem vessel development (von der Mark et al., 2022).

pip5k1 pip5k2 double mutants also display severe protophloem sieve element differentiation failures (Marhava et al., 2020). In developing sieve elements, PIP5K1/2 display a strongly polar, rootward plasma membrane association, which is conferred by interaction with a 'molecular rheostat' composed of BREVIS RADIX (BRX) and the AGC kinase PROTEIN KINASE ASSOCIATED WITH BRX (PAX) (Marhava et al., 2020; Wang et al., 2023). Together, the three proteins form an interdependent self-reinforcing polarity module that regulates auxin efflux and responds itself to auxin. Briefly, the current model suggests that BRX inhibits PAX-mediated auxin efflux activation at low cellular auxin levels, while the recruitment of PIP5K reinforces PAX localization because PI(4,5)P2 promotes PAX polarity (Barbosa et al., 2016). Upon rising auxin levels, PAX activity is potentiated by 3-phosphoinositide-dependent protein kinase (PDK)-mediated phosphorylation (Marhava et al., 2018; Xiao and Offringa, 2020). Subsequently, PAX activates auxin efflux by phosphorylating PINs as well as BRX, the latter is consequently displaced from the plasma membrane (Marhava et al., 2018; Koh et al., 2021; Wang et al., 2023). Because BRX is required for efficient PIP5K recruitment, and because cellular auxin levels drop due to

efflux, the system is eventually reset (Aliaga Fandino and Hardtke, 2022; Wang et al., 2023). The ensuing dynamic equilibrium coordinates auxin flux between adjacent cells to prevent the emergence of fate bistability and leads to auxin canalization in the developing sieve element file (Moret et al., 2020; Aliaga Fandino and Hardtke, 2022).

One cellular output of the self-reinforcing rheostat system is a subcellular PIN pattern that is specific for developing protophloem sieve elements (Marhava et al., 2020). That is, co-localized PIP5K, PAX and BRX association with the center of the rootward plasma membrane in a 'muffin' domain creates a local minimum of PIN abundance which therefore appears as a complementary 'donut' pattern (Fig. 1A). Markers suggest that this central minimum is possibly created by clathrin-mediated PIN endocytosis (Marhava et al., 2020; Wang et al., 2023). In *pax*, *brx* or *pip5k1 pip5k2* mutants, PIN abundance is increased and displays the even 'pancake' distribution (Fig. 1A) throughout the plasma membrane as observed in other cell files (Marhava et al., 2020; Wang et al., 2023). Ultimately, it is BRX-tampered PAX activity that creates the PIN minimum, whereas PIP5K is mainly required to promote PAX polarity in antagonism to sieve element-specific CLAVATA3/EMBRYO SURROUNDING REGION-RELATED 45 (CLE45) peptide signaling through its receptor BARELY ANY MERISTEM 3 (BAM3) (Wang et al., 2023).

Since the protophloem is essential for root meristem maintenance and growth (Anne and Hardtke, 2017), the sieve element differentiation failures in *pax*, *brx* or *pip5k1 pip5k2* mutants are accompanied by a short root phenotype (Marhava et al., 2018; Marhava et al., 2020). Although the observed fate bistability in these loss-of-function backgrounds supports the idea that auxin accumulation is required for sieve element formation (Marhava et al., 2018; Moret et al., 2020), the systemic effects of perturbed protophloem development also obscure the potential role of post-SCN auxin increase in timing the transition to differentiation. Moreover, PAX-mediated PIN control is required for root growth vigor even in the absence of visible protophloem differentiation defects (Wang et al., 2023), raising the question how the tradeoff between PIN activation and PIN abundance plays out. Here we built on the knowledge that auxin accumulation is required for xylem vessel differentiation (von der Mark et al., 2022), and that a spatio-temporal shift in xylem differentiation does not necessarily affect overall root growth

(Ramachandran et al., 2021) to address these issues directly, via a gain-of-function approach in an ectopic context.

Results

PAX-mediated PIN1 phosphorylation promotes PIN1 endocytosis

The interdependence of BRX-PAX-PIP5K module assembly and polarity was previously demonstrated through protophloem sieve element (PPSE)-specific induction of corresponding CITRINE fusion proteins under control of an estradiol-inducible *COTYLEDON VASCULAR PATTERN 2* promoter *($CVP2^{XVE}$)* in reciprocal mutant backgrounds (Wang et al., 2023). Here we used such transgenic lines to determine the impact of the individual components on subcellular PIN patterning, thereby also exploiting the fact that the fusion proteins are by comparison over-expressed upon prolonged induction (Fig. 1B). As previously reported (Wang et al., 2023), PPSE-specific induction of PID, employed as a control, led to a nearly comprehensive PIN1 depolarization (Fig. 1C). PAX induction in *pax* mutant background initially restored the PIN1 'donut-to-pancake' ratio to Columbia-0 (Col-0) wild type levels. Upon prolonged PAX induction, 'donuts' became sharper with a widened PIN1 minimum and even more frequent than in wild type (Fig. 1B and C). By contrast, induced BRX overexpression in *brx* mutant background eventually led to a strong increase in the 'pancake' pattern (Fig. 1B and C). By comparison, prolonged PIP5K1 induction in phenotypically wild type *pip5k2* single mutant background at best slightly increased the 'pancake' frequency (Fig. 1B and C). Collectively, these findings corroborate that PAX is responsible for subcellular PIN 'donut' patterning and that BRX inhibits PAX activity (Marhava et al., 2020; Wang et al., 2023).

AGC kinases phosphorylate several target sites in the hydrophilic loop of PIN proteins, whose combinatorial read-out determines both PIN activity and polarity (Huang et al. 2010, Bassukas et al., 2022). For PAX, several target sites in PIN1 have been described, some of which could be detected with phosphosite-specific anti-PIN1 antibodies (Weller et al., 2017). Two such antibodies were available to us, and we performed immunostainings that corroborated earlier results (Marhava et al., 2018). That is, S271 phosphorylation could still be readily detected in developing PPSEs of *pax* mutants, whereas S231 phosphorylation was essentially absent (Fig. 1D and E). Induction of PAX in *pax* mutant background restored S231 phosphorylation (Supplemental Fig. S2A), suggesting that S231 is a valid PAX target *in vivo* and that PAX is the major kinase for this site in the protophloem. Because PAX induction triggers the appearance of

pronounced PIN1 'donut' patterns and because PAX kinase activity is required for PIN1 patterning (Wang et al., 2023), the data moreover suggest that S231 phosphorylation promotes PIN1 turnover.

Reduced PAX kinase activity also attenuates PIN recycling as revealed by a reduction of PIN1-containing brefeldin-A (BFA) bodies upon BFA treatment (Wang et al., 2023). Together with the observation that DYNAMIN-RELATED PROTEIN 1 A (DRP1A), a promoter of clathrin-mediated endocytosis (Fujimoto et al., 2010), colocalizes with the BRX-PAX-PIP5K 'muffin' domain specifically in developing PPSEs (Dettmer et al., 2014; Marhava et al., 2020), this suggests that the PIN1 minimum may be created by increased local PIN endocytosis. Extended live imaging of developing PPSEs in transgenics expressing an RFP-tagged PIN1 protein simultaneously with either a CITRINE-tagged PAX or BRX protein indeed captured highly dynamic localization of all three proteins, with internalized PIN1 vesicles seemingly originating from the 'muffin' domain (Fig. 2A, Supplemental Fig. S2B). To test the involvement of clathrin-mediated endocytosis in creating the PIN minimum directly, we made transgenic lines for PPSE-specific estradiol-inducible expression of the dominant-negative endocytosis blockers AUXILIN-LIKE 2 (Adamowski et al., 2018) and C-HUB (Kitakura et al., 2011). Indeed, both AUXILIN-LIKE 2 and C-HUB induction triggered a gradual decrease in the PIN1 'donut' pattern and a corresponding increase in the 'pancake' pattern (Fig. 2B-D). In summary, our data support the notion that PAX-mediated PIN1 phosphorylation triggers PIN1 endocytosis to create a local PIN1 minimum.

PAX also patterns subcellular PIN1 distribution in developing xylem vessels

PAX is most prominently expressed in developing PPSEs (Fig. 3A) but also in the xylem axis (Marhava et al., 2018), with a relatively stronger expression in the protoxylem than in the metaxylem (Fig. 3B). Expression of a PAX-CITRINE fusion protein under control of the PPSE-specific *BRX* promoter (Supplemental Fig. S2C) rescued both protophloem differentiation defects as well as diminished root growth of *pax* mutants (Marhava et al., 2018) (Supplemental Fig. S2D and E), suggesting that PAX activity in the developing xylem is not essential for root meristem growth vigor (with the caveat that we cannot exclude weak, below detection threshold xylem expression of PAX). Nevertheless, simultaneous immunolocalization of PAX fusion protein and PIN1 revealed that similar to developing PPSEs, PAX is also localized in a central 'muffin' domain

in developing xylem vessels (Fig. 3C and D). Moreover, in these cells PIN1 also frequently displayed a less defined 'donut' pattern with a smaller yet recognizable minimum (Fig. 3E) that was not observed in other cell files where PAX was undetectable. In the developing xylem of *pax* mutants, the abundance of this pattern was substantially reduced (Fig. 3F-H). Moreover, live imaging of PIN1 fusion protein signal in the plasma membrane of individual cells over time revealed that PIN1 turnover in developing metaxylem vessels is nearly as dynamic as in developing PPSEs (Supplemental Fig. S3A). Unlike in neighboring procambial cell files that displayed overall lower PIN1 turnover, PIN1 dynamics were strongly reduced in developing PPSEs of *pax* mutants (Supplemental Fig. S3A). In summary, our results suggest that even relatively low amounts of PAX can generate a weak yet recognizable PIN1 'donut' pattern in developing xylem vessels.

BRX antagonizes PAX-mediated PIN1 patterning

Unlike PAX, BRX is not detectable outside developing PPSEs (Marhava et al., 2018) and consistently, *brx* mutants did not show a change in the abundance of xylem vessel PIN1 'donuts' (Fig. 3I). Likewise, components of the CLE45 signaling pathway, which interferes with PAX polarity and thereby PIN1 patterning in developing PPSEs (Wang et al., 2023) (Supplemental Fig. S3B), are not expressed in the xylem (Kang and Hardtke, 2016; Breda et al., 2019), and consistently CLE45 treatments did not impact subcellular PIN1 patterning in developing metaxylem vessels (Supplemental Fig. S3C). Thus, the developing xylem is an ideal tissue to probe the functioning of the BRX-PAX-PIP5K module and its cellular impact.

To ectopically assemble the module, we first expressed a BRX-CITRINE fusion protein under control of the *PAX* promoter. As expected, this construct complemented the *brx* PPSE differentiation defects (Supplemental Fig. S4A) and root growth phenotype (Fig. 4A). Although *BRX* expression in the *PAX* domain thus had no detrimental effect *per se*, it interfered with the root growth rescue normally conferred by a *PAX:PAX-CITRINE* transgene in *pax* single mutants (Supplemental Fig. S4B). This was observed in trans-heterozygous *brx +/- pax +/-* background (Fig. 4B), confirming a gain-of-function effect. Importantly, compared to endogenous PAX protein, PAX-CITRINE fusion protein was always expressed at higher levels in developing xylem (Fig. 4C), possibly because of transgene concatenation. However, by itself this did not result in

more frequent or more accentuated PIN1 minima (Fig. 3H). In contrast, additional BRX fusion protein expression in the xylem disrupted subcellular PIN1 patterning and led to an increase in the 'pancake' configuration (Fig. 4D-F), which is again consistent with BRX being an inhibitor of PAX activity (Marhava et al., 2018). In summary, we found that ectopic expression of BRX in developing xylem vessels interfered with root elongation and correlated with an increase in the PIN1 'pancake' pattern when combined with elevated PAX fusion protein levels.

PIP5K1 dampens PAX inhibition by BRX

Similar to PAX, PIP5K1 and PIP5K2 are both expressed in the developing xylem vasculature albeit at barely detectable levels (von der Mark et al., 2022) (Supplemental Fig. S4C and D), even though the PIP5K1-CITRINE fusion protein is sufficient to rescue the *pip5k1 pip5k2* double mutant (Wang et al., 2023). Unlike PAX however, PIP5K localization in the xylem is not polar, and moreover not only plasma-membrane-associated but also nuclear PIP5K1 is required for proper xylem differentiation (von der Mark et al., 2022). The pronounced polar localization of PIP5K1 in developing PPSEs largely depends on the presence of BRX (Marhava et al., 2020; Wang et al., 2023), and indeed PIP5K1-mCHERRY fusion protein that was expressed in the *PAX* expression domain simultaneously with BRX-CITRINE fusion protein displayed a markedly polar enrichment in the xylem (Supplemental Fig. S4E) [but not without BRX-CITRINE (Supplemental Fig. S4F and G)]. Moreover, the PIP5K1 dosage increase partially reversed the negative impact of BRX dosage increase on PAX activity, as indicated by partially recovered root growth (Fig. 4B) and largely restored PIN1 patterning (Fig. 4F and G).

Because PDK1 is expressed in the xylem (Xiao and Offringa, 2020) (Supplemental Fig. S4H), we also monitored auxin-induced plasma-membrane-dissociation of ectopically expressed BRX. In the *brx* mutant background, BRX-CITRINE fusion protein expressed under control of the *PAX* promoter displayed the expected decrease in plasma-membrane-association in PPSEs but not in metaxylem (Supplemental Fig. S4I). However, the response in PPSEs was 'sharpened' (i.e. less variable) by a PAX dosage increase and could then also be observed in the metaxylem (Supplemental Fig. S4I). Thus, the BRX auxin response described for the protophloem (Marhava et al., 2018) could be reconstituted in the xylem. Similar to the other characteristics we had quantified, additional PIP5K1 dampened this response (Supplemental Fig. S4I). Finally, consistent

with our observations, PIN1 S231 phosphorylation was strongly reduced when BRX was introduced into the xylem, but recovered by additional PIP5K1 (Fig. 4H). In summary, these findings reiterate the importance of S231 phosphorylation for the creation of the PIN1 minimum, the positive effect of PIP5K1 on PAX activity, and the intricate quantitative and dosage-sensitive relation between the three module components (Aliaga Fandino and Hardtke, 2022; Wang et al., 2023).

Ectopic assembly of the PAX-BRX-PIP5K1 module changes the developmental trajectory of xylem cells

The PAX-BRX-PIP5K module has an important role in guiding the transition of developing PPSEs towards differentiation (Marhava et al., 2018; Marhava et al., 2020; Moret et al., 2020), and we thus sought to investigate whether the observed gain-of-function effects were associated with altered developmental trajectories of the xylem. The secondary cell wall pattern is an easily scorable morphological indicator of xylem vessel differentiation status and also distinguishes protoxylem vessels with their reticulated pattern from metaxylem vessels with their pitted pattern (Ramachandran et al., 2021).

First, we monitored xylem vessel patterns in the post-meristematic region of roots, between 5 to 7 mm from the tip. As expected (Graeff and Hardtke, 2021), in this area protoxylem vessels were always differentiated whereas metaxylem vessels showed some variation between genotypes (Fig. 5A). In wild type, we always observed two differentiated protoxylem vessels, two differentiated outer metaxylem vessels, and with very few exceptions an undifferentiated central metaxylem vessel (Fig. 5A and B). In *pax* mutants, the central metaxylem had often already differentiated and occasionally an additional xylem cell file was observed (Fig. 5A and C), and this phenotype could be complemented by a *PAX:PAX-CITRINE* transgene (Fig. 5A and D). Thus, PAX loss-of-function may confer a weak xylem phenotype, which however may also simply be related to its short root phenotype because similar aberrations were observed in *brx* mutants (Supplemental Fig. S5A). Addition of a *PAX:BRX-CITRINE* transgene to the *PAX:PAX-CITRINE* transgene led to more frequent changes in xylem cell file number (Fig. 5A and E) and was accentuated by a *PAX:PIP5K1-CITRINE* transgene (Fig. 5A and F). Compared to wild type, in the latter triple transgenic we also frequently observed differentiated metaxylem (Fig. 5F).

Next, we inspected protoxylem differentiation, which occurs closer to the root tip and can be traced continuously from the SCN (Graeff and Hardtke, 2021; Ramachandran et al., 2021). In wild type, *pax* mutants or complemented *pax* mutants we did not observe a statistically significant difference in the onset of protoxylem differentiation with respect to the distance from the SCN (Fig. 5G). However, protoxylem vessels appeared to differentiate closer to the SCN both when BRX, or BRX and PIP5K1 were combined with increased PAX dosage (Fig. 5G). However, unlike in the triple transgenic situation (PAX + BRX + PIP5K1), in the double transgenics (PAX + BRX) we also observed shorter protoxylem cells (Fig. 5H). Finally, we found significantly fewer protoxylem precursor cells in lines expressing the entire PAX-BRX-PIP5K1 module but not in the other genotypes (Fig. 5I). By contrast, no differences were observed in the number of PPSE precursors (Supplemental Fig. S5B). Thus, ectopic expression of BRX in the xylem together with a PAX dosage increase resulted in overall shorter cells but did not accelerate the trajectory of protoxylem differentiation, whereas ectopic expression of the entire PAX-BRX-PIP5K1 module did. In summary, our data indicate that manipulation of PAX activity in the xylem can alter its developmental trajectory.

Ectopic assembly of the PAX-BRX-PIP5K1 module impacts cellular auxin response

Consistent with the morphological observations, *ARABIDOPSIS HISTIDINE PHOSPHOTRANSFER PROTEIN 6 (AHP6)*, a key promoter of protoxylem formation (Mahonen et al., 2006; Moreira et al., 2013), *INDOLE-3-ACETIC ACID INDUCIBLE 19 (IAA19)*, a xylem-expressed auxin-inducible gene (Muto et al., 2007), and *VASCULAR RELATED NAC-DOMAIN PROTEIN 7 (VND7)*, an auxin-responsive master regulator of xylem differentiation (Yamaguchi et al., 2011; Hirai et al., 2019; von der Mark et al., 2022) were significantly upregulated in plants expressing the entire module as determined by RT-qPCR (Fig. 6A and B). Such differential expression was not observed with several other genes, including *ARABIDOPSIS THALIANA HOMEOBOX GENE 8 (ATHB8)*, a promoter of procambial cell fate, or *VND6*, a redundant yet not auxin-responsive *VND7* homolog (Kubo et al., 2005; Ramachandran et al., 2021) (Fig. 6C).

The PAX-BRX-PIP5K module has an important role in guiding the transition of developing PPSEs towards differentiation (Marhava et al., 2020), which has been correlated with timely auxin accumulation (Marhava et al., 2018; Moret et al., 2020; Aliaga Fandino and Hardtke, 2022).

In developing PPSEs of *brx* mutants, auxin levels as determined by the DII-VENUS reporter are generally lower and more variable than in wild type (Marhava et al., 2018), and here we consistently found the same for *pax* mutants (Supplemental Fig. S6A and B). Moreover, auxin levels were also reduced in developing metaxylem vessels (Supplemental Fig. S6C and D), which may reflect the systemic impact of perturbed protophloem development (Anne and Hardtke, 2017). To investigate whether a module gain-of-function affects auxin activity, we crossed combinations of our transgenes with the transcriptional *DR5:NLS-VENUS* auxin reporter line (Heisler et al., 2005). These plants displayed the same root phenotypes observed earlier, confirming the dominant effects. Moreover, compared to the control (*DR5:NLS-VENUS* crossed to *PAX:PAX-CITRINE* in *pax* background), auxin activity was strongly reduced in the developing xylem of PAX + BRX double transgenics (Fig. 6D-E), whereas auxin response appeared to be stronger in PAX + BRX + PIP5K1 triple transgenics (Fig. 6F). Moreover, a stronger auxin response persisted farther proximally in the xylem of PAX + BRX + PIP5K1 triple transgenics (Supplemental Fig. S6E and F). These observations show that ectopic assembly of the PAX-BRX-PIP5K1 module in developing xylem vessels alters cellular auxin activity, likely by its impact on trans-cellular auxin flux.

Discussion

PIN-mediated auxin efflux is subject to complex regulatory inputs, among which targeted PIN recycling and activation are most prominent (Kleine-Vehn et al., 2011; Adamowski and Friml, 2015; Barbosa et al., 2018). AGC kinases play a key role in these processes, through phosphorylation of PIN proteins in their cytoplasmic hydrophilic loop, which is for example necessary for PIN-mediated auxin efflux in the heterologous *Xenopus laevis* oocyte system (Zourelidou et al., 2014; Weller et al., 2017). Several experimentally verified PIN phosphosites have been described and their combinatorial state in a yet to be fully understood 'phosphocode' may determine the overall activity and turnover of PINs (Bassukas et al., 2022). Despite their generally close phylogenetic relation and structural similarity (Galvan-Ampudia and Offringa, 2007), AGC kinases have diverged in their effects on PIN activity. For example, although both PID- and D6PK-mediated PIN phosphorylation promotes auxin efflux in the oocyte system (Zourelidou et al., 2014; Weller et al., 2017), *in planta* PID, but not D6PK, also triggers PIN re-

localization through transcytosis that competes with basal endocytic PIN recycling (Kleine-Vehn et al., 2009; Dhonukshe et al., 2010; Weller et al., 2017). Similar to PID and D6PK, PAX can stimulate PIN-mediated auxin efflux in the oocyte system, but compared to those other kinases it is a relatively weak activator (Marhava et al., 2018). However, a phosphomimic PAX version that simulates the auxin-stimulated PAX phosphorylation by PDKs is not only a much stronger activator of auxin efflux in the oocyte system, but also hyperactive *in planta* (Marhava et al., 2018; Xiao and Offringa, 2020). Finally, what sets PAX apart from the other kinases in its family is its unique N-terminus (Galvan-Ampudia and Offringa, 2007), which was recently shown to be necessary for interaction with PIP5K (Wang et al., 2023). Here we found that *in planta*, PIP5K recruitment dampens PAX inhibition by BRX as demonstrated by phenotypic read-outs as well as cellular features, notably S231 phosphorylation of PIN1. Our data reiterate that PIP5K promotes PAX activity (Wang et al., 2023), and suggest that S231 phosphorylation of PIN1 by PAX not only stimulates PIN1 activity, but also triggers PIN1 endocytosis and subsequent turnover. Moreover, we found that unlike PID, PAX cannot induce PIN re-localization. This may be related to the fact that (ectopically expressed) PID is largely apolar in PPSEs (Wang et al., 2023), whereas PAX remains polar localized even upon prolonged induction. In summary, our results suggest that PAX control of PIN activity is fundamentally distinct from both PID and D6PK due to its unique N-terminus, which allows interaction with PIP5K.

Nevertheless, also in the ectopic xylem context, efficient PIP5K recruitment to the PIN domain requires BRX. Our data thus reiterate that PAX activity depends on its intricate quantitative relationship with both BRX and PIP5K (Marhava et al., 2020; Wang et al., 2023). Until now, the collective, dynamic steady-state output of this three-protein module remained unclear however, because whereas the oocyte assays suggested that PAX kinase activity primarily stimulates PIN-mediated auxin efflux (Marhava et al., 2018; Koh et al., 2021), the PAX-dependent PIN abundance minimum, the 'donut' pattern, suggested that PAX kinase activity may also reduce PIN-mediated auxin efflux (Marhava et al., 2020; Wang et al., 2023). Our results suggest that the two processes could also be intricately linked. Thus, PAX-mediated PIN1 phosphorylation may transiently stimulate auxin efflux but also promote its eventual reset through PIN internalization. This would reconcile a rheostat function that coordinates auxin

levels between adjacent cells along a file with a canalization function that nevertheless promotes auxin accumulation in those cells as compared to their lateral neighbors.

Expression of the PAX-BRX-PIP5K1 module in the developing xylem allowed us to monitor the output of these proposed dynamics in an ectopic context in wild type background and in the absence of CLE45-BAM3 signaling, which interferes with module assembly in developing PPSEs (Diaz-Ardila et al., 2023; Wang et al., 2023). Monitoring of an auxin activity reporter indicates that expression of the PAX-BRX rheostat suppresses auxin accumulation in the developing xylem. Given the systemic importance of xylem-derived auxin for root meristem development (Bishopp et al., 2011), this may explain the short root phenotype and shorter xylem cells of the pertinent transgenic lines. By contrast, ectopic assembly of the entire PAX-BRX-PIP5K module results in higher auxin activity likely due to an overall net auxin retention, which correlates with enhanced PIN patterning (i.e. lower PIN abundance) and an accelerated trajectory of xylem vessel differentiation. Consistently, we found upregulation of genes related to xylem differentiation. Although our method (RT-qPCR) could not exclude that such upregulation reflects ectopic rather than native xylem expression, overall our findings are consistent with the relatively lower auxin levels we observed in the xylem of *pax* mutants, and the recent demonstration that xylem vessel differentiation requires auxin accumulation (von der Mark et al., 2022). Thus, in summary our observations suggest that the PAX-BRX-PIP5K1 module promotes cellular auxin retention and thereby promotes the timely differentiation of developing PPSEs (Marhava et al., 2018; Moret et al., 2020). Since this property can be transferred to the ectopic xylem context, our results also support the notion that the renewed increase of cellular auxin generally observed with reporters after the meristematic cell proliferation stage (Santuari et al., 2011; Brunoud et al., 2012) is likely a generic cue for the timing of differentiation across root tissues.

Materials and Methods

Plant materials and growth conditions

Arabidopsis (*Arabidopsis thaliana*) accession Columbia-0 (Col-0) was the wild type background for all lines used or produced in this study. The following mutant lines and transgenes have been described previously: *brx* (Rodrigues et al., 2009); *pax* and *PAX:PAX-CITRINE* (Marhava et al., 2018); *BRX:BRX-CITRINE* (Rodriguez-Villalon et al., 2014); *CVP2^{XVE}:PAX-CITRINE*, *CVP2^{XVE}:BRX-CITRINE*, *CVP2^{XVE}:PIP5K1-CITRINE* and *CVP2^{XVE}:PID-CITRINE* (Wang et al., 2023), *DR5:NLS-VENUS* (Heisler et al., 2005), *35S:mDII-VENUS* and *35S:DII-VENUS* lines in Col-0 and *brx* (Santuari et al., 2011; Brunoud et al., 2012; Marhava et al., 2018).

Growth conditions

Seeds of Arabidopsis were surface sterilized and then stratified for 2 days in the dark at 4°C before germination and growth in continuous white LED light of c. 120 μE intensity at 22°C on vertically placed Petri dishes that contained 0.5× Murashige and Skoog (MS) media supplemented with 0.8% (w/v) agar and 0.3% (w/v) sucrose.

Root and protophloem phenotyping

Root length was determined by analysis of high resolution flatbed scans of seedlings on tissue culture plates using Fiji software. For quantification of sieve element strand gaps, root protophloem was inspected by confocal microscopy after fixation as previously described (Marhava et al., 2020). For quantification of PIN1 patterns, 3D reconstructions of confocal image stacks were analyzed cell-by-cell in the tissue of interest and classified subjectively as 'donut' or 'pancake' as described in the text.

Constructs and generation of transgenic lines

Transgenes for plant transformation were created in suitable binary vectors using standard molecular biology procedures. For the *PAX:BRX-CITRINE* and *PAX:PIP5K1-mCHERRY* constructs, the *PAX* promoter region (Marhava et al., 2018) was amplified and cloned into pDONR P4P1R. The genomic fragments of the *PIP5K1* and *BRX* transcript regions, without their STOP codons, were amplified and cloned into pDONR 221. These entry clones together with CITRINE or 2xmCHERRY in pDONR P2RP3 were combined into the destination vector pH7m34GW by the

multisite Gateway recombination system. To generate the inducible *CVP2^{XVE}:C-HUB-CITRINE* and *CVP2^{XVE}:AUXILINE-LIKE2-CITRINE* fusions, the *CVP2^{XVE}* promoter (Wang et al., 2023) region was amplified and cloned into pDONR P4P1R, the *AUXILINE-LIKE2* (At4g12770) (Adamowski et al., 2018) and C-HUB (Dhonukshe et al., 2007) coding sequences without their STOP codons were cloned into pDONR 221 and the CITRINE coding sequence into pDONR P2RP3. These entry clones were combined into binary vector pH7m34GW. The binary constructs were introduced into *Agrobacterium tumefaciens* strain GV3101 pMP90 and transformed into the pertinent Arabidopsis genotypes using the floral dip method. For the *35S:mDII-VENUS* and *35S:DII-VENUS* lines in *pax* mutant, the two constructs in Col-0 background were crossed into *pax* and selected by genotyping. For transgene combinations, *PAX:PAX-CITRINE* in *pax* background and *PAX:BRX-CITRINE* with or without *PAX:PIP5K1-mCHERRY* in *brx* background were crossed to create hemizygous F1 plants.

Auxin treatments

To monitor auxin response of BRX, 5-day-old seedlings were transferred into liquid MS media with mock or 10µM auxin (1-naphthylacetic acid dissolved in DMSO). Seedlings were removed for analysis after 3h.

Estradiol treatments

To induce effectors expressed under control of the *CVP2^{XVE}* promoter, 5-day-old seedlings were transferred onto plates of ½ MS media supplemented with 5 µM estradiol. Seedlings were removed for analysis at indicated time points.

Confocal imaging and image processing

Confocal microscopy was performed on *Leica Stellaris 5* and *Zeiss LSM 880 with Airyscan* inverted confocal scanning instruments. To visualize reporter genes and staining signals, the following fluorescence excitation-emission settings were used: CITRINE excitation 514 nm, emission 529 nm; VENUS excitation 515 nm, emission 528 nm; propidium iodide excitation 536 nm, emission 617 nm; Alexa Fluor 488 excitation 498 nm, emission 520 nm; Alexa Fluor 546 excitation 556 nm, emission 573 nm; calcofluor white excitation 405 nm, emission 425–475 nm. Pictures were taken with 20× or 40× water/oil immersion objectives. For presentation, composite images had to be assembled in various instances. Sequential scanning was used for

co-localization studies to avoid interference between fluorescence channels. For image analyses, *ImageJ*, *Zeiss Zen 2011 (black edition)*, and *Imaris* image analysis software were used.

Protein immunolocalization

Whole mount immunolocalization in 5-day-old seedlings was performed as described (Marhava et al., 2020; Wang et al., 2023). Briefly, seedlings were fixed under vacuum in 4 % (w/v) paraformaldehyde (dissolved in MTSB: 15 gl^{-1} PIPES, 1.9 gl^{-1} EGTA, 1.32 gl^{-1} MgSO4·7 H2O, and 5 gl^{-1} KOH, adjusted to pH 6.8-7.0 with KOH) supplemented with 0.1 % (v/v) Triton for 50 min. Samples were then washed 3x with MTSB/0.1% Triton and 2x with water for 10 min. For cell wall digestion, samples were treated for 30 min with 2% (w/v) driselase in MTSB at 37°C. After washing with MTSB, samples were treated 2x for 30 min. with permeabilization solution (10% (v/v) DMSO and 3% (v/v) NP-40 in MTSB). Next, samples were washed 5x with MTSB, pre-incubated in 2% (w/v) BSA in MTSB for 1 h, and incubated with primary antibody for 4 h at 37°C, then with secondary antibody for 3 h at 37°C. After each antibody treatment, samples were washed 5-7x with MTSB for 10-15 min. Samples were mounted in Citi-fluor antifade mounting medium and imaged by confocal laser-scanning microscopy. Separation of individual cells, if desired, was achieved by applying light thumb pressure on slides before imaging. The primary antibody dilutions were: 1:500 for anti-GFP mouse (Roche, 11814460001); 1:600 for anti-GFP rabbit (Abcam, ab290); 1:500 for anti-BRX rabbit (custom, Marhava et al., 2018); 1:250 for anti-PIN1 goat (Santa Cruz, SC27163); 1:100 for anti-PIN1 J231 rabbit (custom, Weller et al., 2017); 1:300 for anti-PIN1 J271 rabbit (custom, Weller et al., 2017); 1:500 for anti-PAX rabbit (custom, Marhava et al., 2018). The secondary antibody dilutions were: 1:500 for Alexa Fluor 488 anti-mouse (Invitrogen, A28175); 1:500 for Alexa Fluor 546 anti-rabbit (Invitrogen, A10040); 1:500 for Alexa Fluor 546 anti-goat (Invitrogen, A11056).

RT-qPCR

For expression analysis, ca. 7mm of the root tip from 7-day-old seedlings of each genotype were collected. Total RNA was extracted using an RNeasy Plant Mini Kit (QIAGEN) and treated with Dnase I on the column. cDNA was synthesized with the SuperScriptII kit (Invitrogen) and used as a template for qPCR assays with the MESA BLUE kit (Takyon), using the primers listed in Supplemental Table S1. The relative expression values were calculated using the *ACTIN 7* gene as

a reference, using the ΔΔCT method. All assays were performed with three technical replicates each of three biological replicates.

Xylem differentiation quantification

To analyze xylem differentiation status, roots were mounted in chloralhydrate solution (8:2:1 chloralhydrate:glycerol:water w/v/v), and visualized on a *Leica* light microscope with differential interference contrast optics. To score trajectories in the meristem, 6-day-old plants were fixed in 4% (w/v) PFA, washed 4x in MTSB, and cleared overnight in ClearSee solution. The next day samples were placed in a basic fuchsin-ClearSee mixture (final basic fuchsin concentration 0.2% (v/v) in ClearSee) overnight. The following day the samples were washed 2x for 1 h in ClearSee and mounted on slides with ClearSee for visualization on the *Leica Thunder* microscope. To count protoxylem precursors from the QC to the first differentiated protoxylem vessel, samples from anti-PIN1 immunolocalization were used to distinguish cell boundaries.

Statistical analyses

Analyses to determine statistical significance were performed in Graphpad Prism software, version 9.3.1. Specific statistical tests used (Student's *t*-test, Fisher's exact test, ordinary one-way ANOVA followed by Tukey's multiple comparisons test) are indicated in the figure legends and were always two-tailed. Robust regression and outlier removal (ROUT) analyses were performed on discrete measurements to detect (rare) outliers, which were removed. All experiments were replicated at least twice, typically three times. Statistical data are provided in Supplemental Data Set S1.

Accession numbers

Sequence data from this article can be found in the GenBank/EMBL data libraries under the following accession numbers: At2g44830 (PAX); At1g31880 (BRX); AT1G21980 (PIP5K1); and AT5G04510 (PDK1).

Data availability

This study includes no data deposited in external repositories.

Funding information

This study was funded by a bilateral grant between the *Swiss National Science Foundation* (SNF) and the *Czech Science Foundation* (CSF) (SNF grant 310030L_197794 awarded to C.S.H. and CSF grant 21-08021L awarded to J.P.). A.C.A.F. was supported by a Ph.D. Fellowship from the Faculty of Biology and Medicine of the University of Lausanne.

Acknowledgments

We would like to thank Prof. N. Geldner for comments on the manuscript, Prof. C. Schwechheimer for a gift of phosphosite-specific anti-PIN1 antibodies, Prof. R. Offringa for PDK-related materials, and the Imaging Facility of the Institute of Experimental Botany at the Czech Academy of Sciences and the Cellular Imaging Facility at the University of Lausanne for microscopy support.

Author contributions

Conceptualization A.C.A.F and C.S.H.; Methodology A.C.A.F., A.J. and P.M.; Investigation A.C.A.F., A.J. and P.M.; Validation A.C.A.F., A.J. and P.M.; Visualization A.C.A.F., A.J. and P.M.; Writing – Original Draft A.C.A.F. and C.S.H.; Writing – Review & Editing A.C.A.F., A.J., P.M., J.P. and C.S.H.; Funding Acquisition J.P. and C.S.H.; Supervision J.P. and C.S.H.

Disclosure and competing interests statement

The authors declare no competing interests.

Figure legends

Figure 1. PAX targets a specific PIN1 phosphosite in developing protophloem sieve elements (PPSEs).

(A) Confocal microscopy live images of PIN1-RFP, PAX-CITRINE and PIN1-GFP fusion proteins at the rootward plasma membrane of a developing PPSE with signal intensity traces along the central lines, illustrating the peripheral 'donut' pattern of PIN1 that is complementary to the central 'muffin' localization of PAX and transformed into a 'pancake' pattern in *pax* mutant background.

(B) Simultaneous detection of PIN1 (anti-PIN1 antibody, red fluorescence) and CITRINE fusion proteins (anti-GFP antibody, yellow fluorescence) by immunostaining. Transgenic plants expressing the indicated fusion proteins under control of the PPSE-specific estradiol-inducible *COTYLEDON VASCULAR PATTERN 2* promoter ($CVP2^{XVE}$) were transferred onto estradiol media and monitored at indicated timepoints. Asterisks highlight the PPSE cell file (calcofluor white staining, grey fluorescence).

(C) Quantification of the subcellular PIN1 pattern in developing PPSEs, corresponding to (B). n=76-217 PPSEs per time point; statistically significant differences (lower case letters) were determined by Chi square test, $p<0.001$.

(D-E) Simultaneous detection of transgenic PIN1-GFP fusion protein (anti-GFP antibody, yellow fluorescence) with either anti-PIN1, or $S231^{P}$-phosphosite-specific anti-PIN1, or $S271^{P}$-

phosphosite-specific anti-PIN1 antibodies (red fluorescence) by immunostaining in Columbia-0 (Col-0) wild type (D) or *pax* mutant (E) background.

Figure 2. The central minimum in developing protophloem sieve elements (PPSEs) reflects enhanced PIN1 endocytosis.

(A) Time course of PIN1-RFP (magenta fluorescence) and PAX-CITRINE (green fluorescence) fusion protein dynamics at the rootward plasma membrane of a developing PPSE, capturing PIN1-RFP internalization from the center (highlighted by white arrowheads in the merged sequence).

(B-C) Simultaneous immunostaining of PIN1 (anti-PIN1 antibody, red fluorescence) and CITRINE fusions (anti-GFP antibody, yellow fluorescence) with dominant inhibitors of clathrin-mediated endocytosis. Transgenic plants expressing either AUXILIN-LIKE 2 (B) or C-HUB (C) fusion protein under control of the $CVP2^{XVE}$ promoter were monitored before and after transfer onto estradiol media. 3D reconstructions of PIN1 and corresponding top-down views on the rootward end of individual vessels are shown aside merged views with the induced effectors. Asterisks highlight the PPSE cell file (calcofluor white staining, grey fluorescence).

(D) Quantification of the subcellular PIN1 pattern in developing PPSEs, corresponding to (B) and (C). n=140-153 PPSEs per time point; statistically significant differences (lower case letters) were determined by Fisher's exact test, $p<0.0001$.

Figure 3. PAX expression in the xylem and corresponding subcellular PIN1 pattern.

(A-B) Confocal live imaging of PAX-CITRINE fusion protein (yellow fluorescence, left panels) expressed under control of its native promoter in *pax* mutant background, and merged with propidium iodide cell wall staining (red fluorescence, center panels). Longitudinal optical sections through the protophloem (A) and xylem axis (B) planes are shown. Vascular cell types indicated by arrows in the magnified images (right panels) are color-coded with reference to the schematic overviews.

(C-D) Simultaneous detection of PIN1 (anti-PIN1 antibody, red fluorescence) and PAX-CITRINE fusion protein (anti-GFP antibody, yellow fluorescence) by immunostaining, shown in longitudinal (C) and horizontal (D) view 3D reconstructions.

(E) Examples of PIN1 'donut' and 'pancake' subcellular patterning in developing metaxylem vessels, detected by anti-PIN1 antibody staining.

(F-G) Detection of PIN1 by anti-PIN1 antibody staining (red fluorescence) in developing metaxylem vessels, showing 3D reconstructions (left panels) and corresponding top-down views on the rootward end of individual vessels (right panels).

(H-I) Quantification of the subcellular PIN1 pattern in developing metaxylem (MX) vessels in indicated genotypes. n=323-483 MX vessels; statistically significant differences (lower case letters) were determined by Fisher's exact test, p=0.0052.

Figure 4. Ectopic expression of the PAX-BRX-PIP5K1 module in developing xylem vessels affects subcellular PIN1 patterning.

(A-B) Primary root length of indicated genotypes. Transgenic PAX and BRX proteins were expressed as CITRINE fusions, PIP5K1 as an mCHERRY fusion. n=41-68 roots (A) and n=39-47 roots (B); statistically significant differences were determined by ordinary one-way ANOVA, p<0.0001 in (A) and (B).

(C) Detection of native PAX in Col-0 wild type or transgenic PAX-CITRINE fusion protein in *pax* mutant background by anti-PAX antibody staining (red fluorescence) in developing protophloem sieve elements (left panels) or metaxylem vessels (right panels). Note the higher expression level of transgenic fusion protein (e.g. white arrows) as compared to endogenous PAX.

(D-E) Simultaneous detection of PIN1 (anti-PIN1 antibody, red fluorescence) and indicated CITRINE fusion proteins (anti-GFP antibody, yellow fluorescence) by immunostaining, shown in longitudinal (') and horizontal ('') overview, and top-down view in individual protoxylem (PX) vessels (''') (3D reconstructions).

(F) Quantification of the subcellular PIN1 pattern in developing metaxylem (MX) vessels in indicated genotypes. n=142-182 MX vessels; statistically significant differences (lower case letters) were determined by Fisher's exact test, p≤0.0202.

(G) As in D-E.

(H) Relative signal intensity of $S231^{P}$-specific PIN1 immunostaining in developing MX vessels of indicated genotypes. n=62-206 MX vessels; statistically significant differences (lower case letters) were determined by ordinary one-way ANOVA, p≤0.0007.

595 Box plots display 2nd and 3rd quartiles and the median, bars indicate maximum and minimum.

596 **Figure 5. Ectopic assembly of the PAX-BRX-PIP5K1 module affects the trajectory of xylem**
597 **development.**

598 (A-F) Differential interference contrast light microscopy example images of the xylem axis in the
599 indicated genotypes, taken 5-7 mm above the root tip (A), and quantification of corresponding
600 differentiation status per vessel type and genotype (B-F). n=22-35 roots.

601 (G) Distance of the first lignified protoxylem vessels from the quiescent center (QC) in the
602 indicated genotypes. n=22-48 roots; statistically significant differences (lower case letters) were
603 determined by ordinary one-way ANOVA, $p \leq 0.0027$.

604 (H) Length of the first lignified protoxylem (PX) vessels in the indicated genotypes. n=17-35 PX
605 vessels; statistically significant differences (lower case letters) were determined by ordinary one-
606 way ANOVA, $p \leq 0.0010$.

607 (I) Number of undifferentiated vessel precursors in PX cell files until the first lignified PX vessel in
608 the indicated genotypes, counted from the QC. n=16-43 cell files; statistically significant
609 differences (lower case letters) were determined by ordinary one-way ANOVA, $p=0.0003$.

610 Box plots display 2nd and 3rd quartiles and the median, bars indicate maximum and minimum.

611 **Figure 6. Ectopic PAX-BRX-PIP5K1 assembly affects xylem differentiation markers and auxin**
612 **activity.**

613 (A-C) qPCR quantification of selected xylem development markers and control genes, normalized
614 with respect to expression of the *ACTIN 2* (*ACT2*) housekeeping gene (A) and expressed as
615 relative fold-change as compared to Col-0 wild type (B-C). Plots display the averages of 3
616 technical replicates from 3 biological replicates each. Statistically significant differences
617 (asterisks) were determined by Student's *t*-test compared to Col-0 wild type, $p<0.001$ (*AHP6*),
618 $p=0.042$ (*IAA19*), $p=0.008$ (*VND7*).

619 (D-F) Confocal microscopy images of the auxin activity reporter *DR5:NLS-VENUS* in the presence
620 of the indicated transgenes after crossing (all transgenes in hemizygous state). Yellow
621 fluorescence: NLS-VENUS (nuclear signal) or PAX/BRX-CITRINE (plasma membrane signal); Red
622 fluorescence: propidium iodide (PI) signal.

623 Box plots display 2nd and 3rd quartiles and the median, bars indicate maximum and minimum.

624

References

Adamowski, M., and Friml, J. (2015). PIN-dependent auxin transport: action, regulation, and evolution. Plant Cell 27, 20-32.

Adamowski, M., Narasimhan, M., Kania, U., Glanc, M., De Jaeger, G., and Friml, J. (2018). A Functional Study of AUXILIN-LIKE1 and 2, Two Putative Clathrin Uncoating Factors in Arabidopsis. Plant Cell 30, 700-716.

Aliaga Fandino, A.C., and Hardtke, C.S. (2022). Auxin transport in developing protophloem: A case study in canalization. J Plant Physiol 269, 153594.

Anne, P., and Hardtke, C.S. (2017). Phloem function and development-biophysics meets genetics. Curr Opin Plant Biol 43, 22-28.

Barbosa, I.C., Zourelidou, M., Willige, B.C., Weller, B., and Schwechheimer, C. (2014). D6 PROTEIN KINASE activates auxin transport-dependent growth and PIN-FORMED phosphorylation at the plasma membrane. Dev Cell 29, 674-685.

Barbosa, I.C., Shikata, H., Zourelidou, M., Heilmann, M., Heilmann, I., and Schwechheimer, C. (2016). Phospholipid composition and a polybasic motif determine D6 PROTEIN KINASE polar association with the plasma membrane and tropic responses. Development 143, 4687-4700.

Barbosa, I.C.R., Hammes, U.Z., and Schwechheimer, C. (2018). Activation and Polarity Control of PIN-FORMED Auxin Transporters by Phosphorylation. Trends Plant Sci 23, 523-538.

Bassukas, A.E.L., Xiao, Y., and Schwechheimer, C. (2022). Phosphorylation control of PIN auxin transporters. Curr Opin Plant Biol 65, 102146.

Bishopp, A., Help, H., El-Showk, S., Weijers, D., Scheres, B., Friml, J., Benkova, E., Mahonen, A.P., and Helariutta, Y. (2011). A mutually inhibitory interaction between auxin and cytokinin specifies vascular pattern in roots. Curr Biol 21, 917-926.

Blilou, I., Xu, J., Wildwater, M., Willemsen, V., Paponov, I., Friml, J., Heidstra, R., Aida, M., Palme, K., and Scheres, B. (2005). The PIN auxin efflux facilitator network controls growth and patterning in Arabidopsis roots. Nature 433, 39-44.

Breda, A.S., Hazak, O., Schultz, P., Anne, P., Graeff, M., Simon, R., and Hardtke, C.S. (2019). A Cellular Insulator against CLE45 Peptide Signaling. Curr Biol 29, 2501-2508 e2503.

Brunoud, G., Wells, D.M., Oliva, M., Larrieu, A., Mirabet, V., Burrow, A.H., Beeckman, T., Kepinski, S., Traas, J., Bennett, M.J., and Vernoux, T. (2012). A novel sensor to map auxin response and distribution at high spatio-temporal resolution. Nature 482, 103-106.

Dettmer, J., Ursache, R., Campilho, A., Miyashima, S., Belevich, I., O'Regan, S., Mullendore, D.L., Yadav, S.R., Lanz, C., Beverina, L., Papagni, A., Schneeberger, K., Weigel, D., Stierhof, Y.D., Moritz, T., Knoblauch, M., Jokitalo, E., and Helariutta, Y. (2014). CHOLINE TRANSPORTER-LIKE1 is required for sieve plate development to mediate long-distance cell-to-cell communication. Nat Commun 5, 4276.

Dhonukshe, P., Aniento, F., Hwang, I., Robinson, D.G., Mravec, J., Stierhof, Y.D., and Friml, J. (2007). Clathrin-mediated constitutive endocytosis of PIN auxin efflux carriers in Arabidopsis. Curr Biol 17, 520-527.

Dhonukshe, P., Huang, F., Galvan-Ampudia, C.S., Mahonen, A.P., Kleine-Vehn, J., Xu, J., Quint, A., Prasad, K., Friml, J., Scheres, B., and Offringa, R. (2010). Plasma membrane-bound AGC3 kinases phosphorylate PIN auxin carriers at TPRXS(N/S) motifs to direct apical PIN recycling. Development 137, 3245-3255.

Diaz-Ardila, H.N., Gujas, B., Wang, Q., Moret, B., and Hardtke, C.S. (2023). pH-dependent CLE peptide perception permits phloem differentiation in Arabidopsis roots. Curr Biol.

Friml, J., Yang, X., Michniewicz, M., Weijers, D., Quint, A., Tietz, O., Benjamins, R., Ouwerkerk, P.B., Ljung, K., Sandberg, G., Hooykaas, P.J., Palme, K., and Offringa, R. (2004). A PINOID-dependent binary switch in apical-basal PIN polar targeting directs auxin efflux. Science 306, 862-865.

Fujimoto, M., Arimura, S., Ueda, T., Takanashi, H., Hayashi, Y., Nakano, A., and Tsutsumi, N. (2010). Arabidopsis dynamin-related proteins DRP2B and DRP1A participate together in clathrin-coated vesicle formation during endocytosis. Proc Natl Acad Sci U S A 107, 6094-6099.

Galvan-Ampudia, C.S., and Offringa, R. (2007). Plant evolution: AGC kinases tell the auxin tale. Trends Plant Sci 12, 541-547.

Gerth, K., Lin, F., Daamen, F., Menzel, W., Heinrich, F., and Heilmann, M. (2017). Arabidopsis phosphatidylinositol 4-phosphate 5-kinase 2 contains a functional nuclear localization sequence and interacts with alpha-importins. Plant J 92, 862-878.

Graeff, M., and Hardtke, C.S. (2021). Metaphloem development in the Arabidopsis root tip. Development 148.

Grieneisen, V.A., Xu, J., Maree, A.F., Hogeweg, P., and Scheres, B. (2007). Auxin transport is sufficient to generate a maximum and gradient guiding root growth. Nature 449, 1008-1013.

Heisler, M.G., Ohno, C., Das, P., Sieber, P., Reddy, G.V., Long, J.A., and Meyerowitz, E.M. (2005). Patterns of auxin transport and gene expression during primordium development revealed by live imaging of the Arabidopsis inflorescence meristem. Curr Biol 15, 1899-1911.

Hirai, R., Higaki, T., Takenaka, Y., Sakamoto, Y., Hasegawa, J., Matsunaga, S., Demura, T., and Ohtani, M. (2019). The Progression of Xylem Vessel Cell Differentiation is Dependent on the Activity Level of VND7 in Arabidopsis thaliana. Plants (Basel) 9.

Huang, F., Zago, M.K., Abas, L., van Marion, A., Galvan-Ampudia, C.S., and Offringa, R. (2010). Phosphorylation of conserved PIN motifs directs Arabidopsis PIN1 polarity and auxin transport. Plant Cell 22, 1129-1142.

Ischebeck, T., Werner, S., Krishnamoorthy, P., Lerche, J., Meijon, M., Stenzel, I., Lofke, C., Wiessner, T., Im, Y.J., Perera, I.Y., Iven, T., Feussner, I., Busch, W., Boss, W.F., Teichmann, T., Hause, B., Persson, S., and Heilmann, I. (2013). Phosphatidylinositol 4,5-bisphosphate influences PIN polarization by controlling clathrin-mediated membrane trafficking in Arabidopsis. Plant Cell 25, 4894-4911.

Kang, Y.H., and Hardtke, C.S. (2016). Arabidopsis MAKR5 is a positive effector of BAM3-dependent CLE45 signaling. EMBO Rep 17, 1145-1154.

Kitakura, S., Vanneste, S., Robert, S., Lofke, C., Teichmann, T., Tanaka, H., and Friml, J. (2011). Clathrin mediates endocytosis and polar distribution of PIN auxin transporters in Arabidopsis. Plant Cell 23, 1920-1931.

Kleine-Vehn, J., Huang, F., Naramoto, S., Zhang, J., Michniewicz, M., Offringa, R., and Friml, J. (2009). PIN auxin efflux carrier polarity is regulated by PINOID kinase-mediated recruitment into GNOM-independent trafficking in Arabidopsis. Plant Cell 21, 3839-3849.

Kleine-Vehn, J., Wabnik, K., Martiniere, A., Langowski, L., Willig, K., Naramoto, S., Leitner, J., Tanaka, H., Jakobs, S., Robert, S., Luschnig, C., Govaerts, W., Hell, S.W., Runions, J., and Friml, J. (2011). Recycling, clustering, and endocytosis jointly maintain PIN auxin carrier polarity at the plasma membrane. Mol Syst Biol 7, 540.

Koh, S.W.H., Marhava, P., Rana, S., Graf, A., Moret, B., Bassukas, A.E.L., Zourelidou, M., Kolb, M., Hammes, U.Z., Schwechheimer, C., and Hardtke, C.S. (2021). Mapping and engineering of auxin-induced plasma membrane dissociation in BRX family proteins. Plant Cell 33, 1945-1960.

Kubo, M., Udagawa, M., Nishikubo, N., Horiguchi, G., Yamaguchi, M., Ito, J., Mimura, T., Fukuda, H., and Demura, T. (2005). Transcription switches for protoxylem and metaxylem vessel formation. Genes Dev 19, 1855-1860.

Lavy, M., and Estelle, M. (2016). Mechanisms of auxin signaling. Development 143, 3226-3229.

Mahonen, A.P., Bishopp, A., Higuchi, M., Nieminen, K.M., Kinoshita, K., Tormakangas, K., Ikeda, Y., Oka, A., Kakimoto, T., and Helariutta, Y. (2006). Cytokinin signaling and its inhibitor AHP6 regulate cell fate during vascular development. Science 311, 94-98.

Mahonen, A.P., Ten Tusscher, K., Siligato, R., Smetana, O., Diaz-Trivino, S., Salojarvi, J., Wachsman, G., Prasad, K., Heidstra, R., and Scheres, B. (2014). PLETHORA gradient formation mechanism separates auxin responses. Nature 515, 125-129.

Marhava, P., Bassukas, A.E.L., Zourelidou, M., Kolb, M., Moret, B., Fastner, A., Schulze, W.X., Cattaneo, P., Hammes, U.Z., Schwechheimer, C., and Hardtke, C.S. (2018). A molecular rheostat adjusts auxin flux to promote root protophloem differentiation. Nature 558, 297-300.

Marhava, P., Aliaga Fandino, A.C., Koh, S.W.H., Jelinkova, A., Kolb, M., Janacek, D.P., Breda, A.S., Cattaneo, P., Hammes, U.Z., Petrasek, J., and Hardtke, C.S. (2020). Plasma Membrane Domain Patterning and Self-Reinforcing Polarity in Arabidopsis. Dev Cell 52, 223-235 e225.

738 Moreira, S., Bishopp, A., Carvalho, H., and Campilho, A. (2013). AHP6 inhibits cytokinin signaling
739 to regulate the orientation of pericycle cell division during lateral root initiation. PLoS
740 One 8, e56370.
741 Moret, B., Marhava, P., Aliaga Fandino, A.C., Hardtke, C.S., and Ten Tusscher, K.H.W. (2020).
742 Local auxin competition explains fragmented differentiation patterns. Nat Commun 11,
743 2965.
744 Morris, D.A., and Kadir, G.O. (1972). Pathways of auxin transport in the intact pea seedling
745 (Pisum sativum L.). Planta 107, 171-182.
746 Muto, H., Watahiki, M.K., Nakamoto, D., Kinjo, M., and Yamamoto, K.T. (2007). Specificity and
747 similarity of functions of the Aux/IAA genes in auxin signaling of Arabidopsis revealed by
748 promoter-exchange experiments among MSG2/IAA19, AXR2/IAA7, and SLR/IAA14. Plant
749 Physiol 144, 187-196.
750 Ramachandran, P., Augstein, F., Mazumdar, S., Nguyen, T.V., Minina, E.A., Melnyk, C.W., and
751 Carlsbecker, A. (2021). Abscisic acid signaling activates distinct VND transcription factors
752 to promote xylem differentiation in Arabidopsis. Curr Biol 31, 3153-3161 e3155.
753 Rodrigues, A., Santiago, J., Rubio, S., Saez, A., Osmont, K.S., Gadea, J., Hardtke, C.S., and
754 Rodriguez, P.L. (2009). The short-rooted phenotype of the brevis radix mutant partly
755 reflects root abscisic acid hypersensitivity. Plant Physiol 149, 1917-1928.
756 Rodriguez-Villalon, A., Gujas, B., Kang, Y.H., Breda, A.S., Cattaneo, P., Depuydt, S., and Hardtke,
757 C.S. (2014). Molecular genetic framework for protophloem formation. Proc Natl Acad Sci
758 U S A 111, 11551-11556.
759 Sabatini, S., Beis, D., Wolkenfelt, H., Murfett, J., Guilfoyle, T., Malamy, J., Benfey, P., Leyser, O.,
760 Bechtold, N., Weisbeek, P., and Scheres, B. (1999). An auxin-dependent distal organizer
761 of pattern and polarity in the Arabidopsis root. Cell 99, 463-472.
762 Santuari, L., Scacchi, E., Rodriguez-Villalon, A., Salinas, P., Dohmann, E.M., Brunoud, G., Vernoux,
763 T., Smith, R.S., and Hardtke, C.S. (2011). Positional information by differential endocytosis
764 splits auxin response to drive Arabidopsis root meristem growth. Curr Biol 21, 1918-1923.
765 Teale, W.D., Paponov, I.A., and Palme, K. (2006). Auxin in action: signalling, transport and the
766 control of plant growth and development. Nat Rev Mol Cell Biol 7, 847-859.

Tejos, R., Sauer, M., Vanneste, S., Palacios-Gomez, M., Li, H., Heilmann, M., van Wijk, R., Vermeer, J.E., Heilmann, I., Munnik, T., and Friml, J. (2014). Bipolar Plasma Membrane Distribution of Phosphoinositides and Their Requirement for Auxin-Mediated Cell Polarity and Patterning in Arabidopsis. Plant Cell 26, 2114-2128.

Vaughan-Hirsch, J., Goodall, B., and Bishopp, A. (2018). North, East, South, West: mapping vascular tissues onto the Arabidopsis root. Curr Opin Plant Biol 41, 16-22.

von der Mark, C., Cruz, T.M.D., Blanco-Tourinan, N., and Rodriguez-Villalon, A. (2022). Bipartite phosphoinositide-dependent modulation of auxin signaling during xylem differentiation in Arabidopsis thaliana roots. New Phytol 236, 1734-1747.

Wang, Q., Aliaga Fandino, A.C., Graeff, M., DeFalco, T.A., Zipfel, C., and Hardtke, C.S. (2023). A phosphoinositide hub connects CLE peptide signaling and polar auxin efflux regulation. Nat Commun 14, 423.

Watari, M., Kato, M., Blanc-Mathieu, R., Tsuge, T., Ogata, H., and Aoyama, T. (2022). Functional Differentiation among the Arabidopsis Phosphatidylinositol 4-Phosphate 5-Kinase Genes PIP5K1, PIP5K2 and PIP5K3. Plant Cell Physiol 63, 635-648.

Weller, B., Zourelidou, M., Frank, L., Barbosa, I.C., Fastner, A., Richter, S., Jurgens, G., Hammes, U.Z., and Schwechheimer, C. (2017). Dynamic PIN-FORMED auxin efflux carrier phosphorylation at the plasma membrane controls auxin efflux-dependent growth. Proc Natl Acad Sci U S A 114, E887-E896.

Willige, B.C., Ahlers, S., Zourelidou, M., Barbosa, I.C., Demarsy, E., Trevisan, M., Davis, P.A., Roelfsema, M.R., Hangarter, R., Fankhauser, C., and Schwechheimer, C. (2013). D6PK AGCVIII kinases are required for auxin transport and phototropic hypocotyl bending in Arabidopsis. Plant Cell 25, 1674-1688.

Xiao, Y., and Offringa, R. (2020). PDK1 regulates auxin transport and Arabidopsis vascular development through AGC1 kinase PAX. Nat Plants 6, 544-555.

Yamaguchi, M., Mitsuda, N., Ohtani, M., Ohme-Takagi, M., Kato, K., and Demura, T. (2011). VASCULAR-RELATED NAC-DOMAIN7 directly regulates the expression of a broad range of genes for xylem vessel formation. Plant J 66, 579-590.

795 Zhao, Y. (2018). Essential Roles of Local Auxin Biosynthesis in Plant Development and in
796 Adaptation to Environmental Changes. Annu Rev Plant Biol 69, 417-435.
797 Zourelidou, M., Absmanner, B., Weller, B., Barbosa, I.C., Willige, B.C., Fastner, A., Streit, V., Port,
798 S.A., Colcombet, J., de la Fuente van Bentem, S., Hirt, H., Kuster, B., Schulze, W.X.,
799 Hammes, U.Z., and Schwechheimer, C. (2014). Auxin efflux by PIN-FORMED proteins is
800 activated by two different protein kinases, D6 PROTEIN KINASE and PINOID. Elife 3.

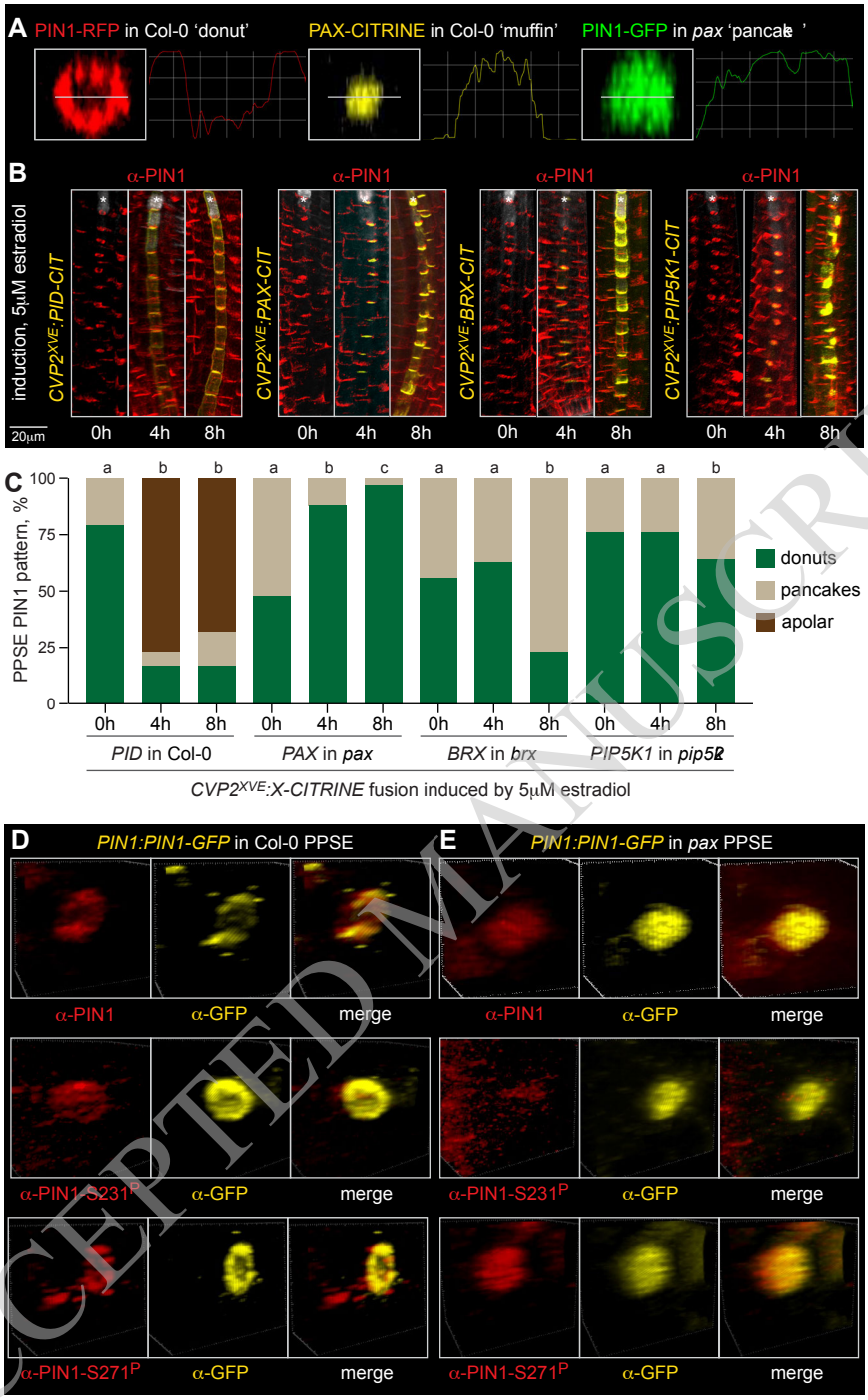

Figure 1. PAX targets a specific PIN1 phosphosite in developing protophloem sieve elements (PPSEs). (A) Confocal microscopy live images of PIN1-RFP, PAX-CITRINE and PIN1-GFP fusion proteins at the rootward plasma membrane of a developing PPSE with signal intensity traces along the central lines, illustrating the peripheral 'donut' pattern of PIN1 that is complementary to the central 'muffin' localization of PAX and transformed into a 'pancake' pattern in *pax* mutant background. (B) Simultaneous detection of PIN1 (anti-PIN1 antibody, red fluorescence) and CITRINE fusion proteins (anti-GFP antibody, yellow fluorescence) by immunostaining. Transgenic plants expressing the indicated fusion proteins under control of the PPSE-specific estradiol-inducible *COTYLEDON VASCULAR PATTERN 2* promoter (*CVP2*^{XVE}) were transferred onto estradiol media and monitored at indicated timepoints. Asterisks highlight the PPSE cell file (calcofluor white staining, grey fluorescence). (C) Quantification of the subcellular PIN1 pattern in developing PPSEs, corresponding to (B). n=76-217 PPSEs per time point; statistically significant differences (lower case letters) were determined by Chi square test, p<0.001. (D-E) Simultaneous detection of transgenic PIN1-GFP fusion protein (anti-GFP antibody, yellow fluorescence) with either anti-PIN1, or S231^{P}-phosphosite-specific anti-PIN1, or S271^{P}-phosphosite-specific anti-PIN1 antibodies (red fluorescence) by immunostaining in Columbia-0 (Col-0) wildtype (D) or *pax* mutant (E) background.

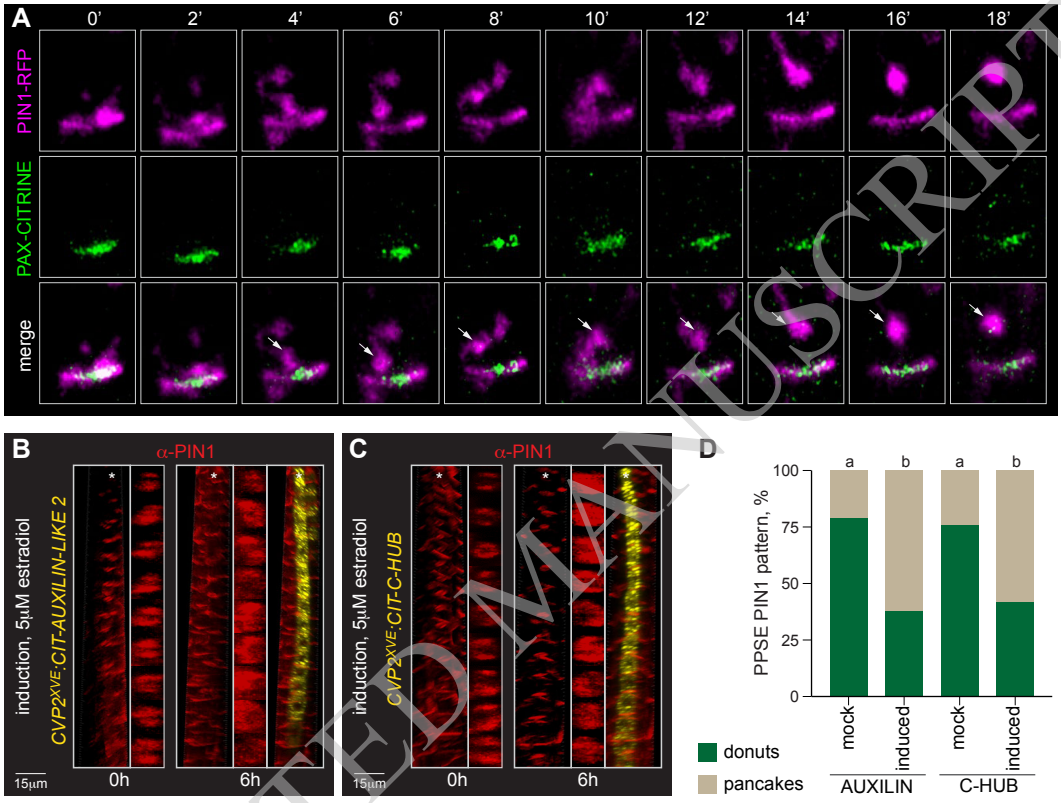

Figure 2. The central minimum in developing protophloem sieve elements (PPSEs) reflects enhanced PIN1 endocytosis. (A) Time course of PIN1-RFP (magenta fluorescence) and PAX-CITRINE (green fluorescence) fusion protein dynamics at the rootward plasma membrane of a developing PPSE, capturing PIN1-RFP internalization from the center (highlighted by white arrowheads in the merged sequence). (B-C) Simultaneous immunostaining of PIN1 (anti-PIN1 antibody, red fluorescence) and CITRINE fusions (anti-GFP antibody, yellow fluorescence) with dominant inhibitors of clathrin-mediated endocytosis. Transgenic plants expressing either AUXILIN-LIKE 2 (B) or C-HUB (C) fusion protein under control of the *CVP2*^{XVE} promoter were monitored before and after transfer onto estradiol media. 3D reconstructions of PIN1 and corresponding top-down views on the rootward end of individual vessels are shown aside merged views with the induced effectors. Asterisks highlight the PPSE cell file (calcofluor white staining, grey fluorescence). (D) Quantification of the subcellular PIN1 pattern in developing PPSEs, corresponding to (B) and (C). n=140-153 PPSEs per time point; statistically significant differences (lower case letters) were determined by Fisher's exact test, $p<0.0001$.

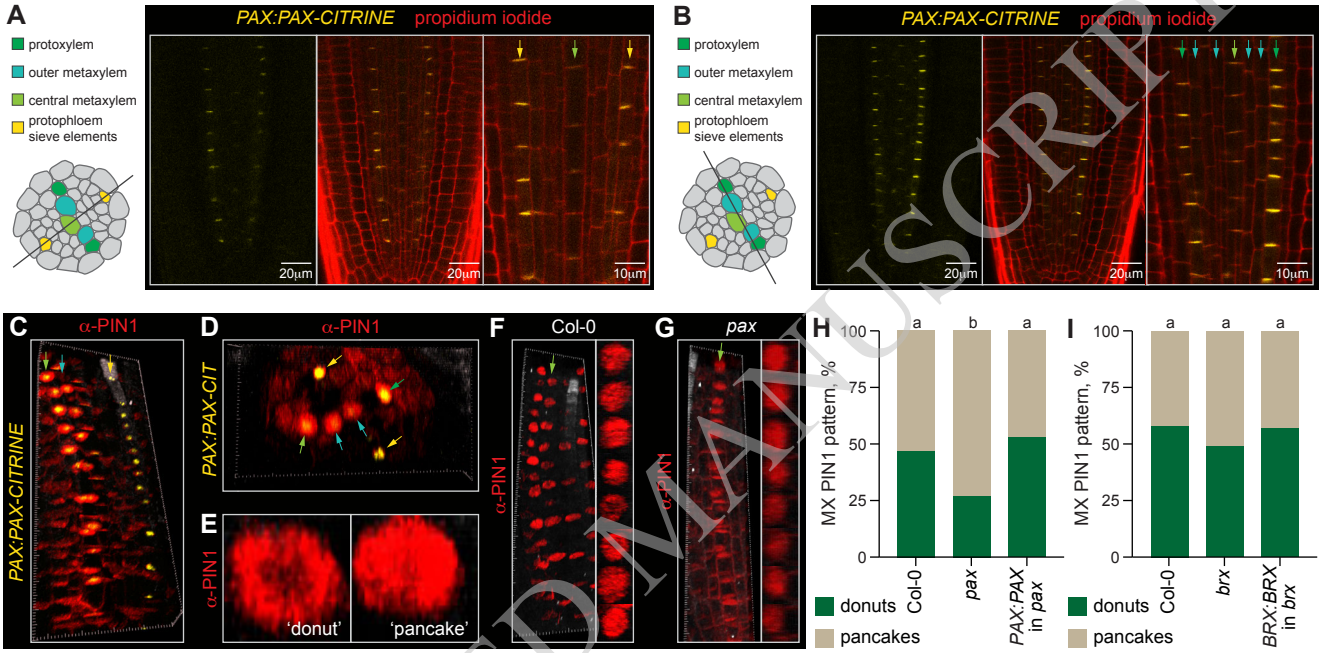

Figure 3. PAX expression in the xylem and corresponding subcellular PIN1 pattern. (A-B) Confocal live imaging of PAX-CITRINE fusion protein (yellow fluorescence, left panels) expressed under control of its native promoter in *pax* mutant background, and merged with propidium iodide cell wall staining (red fluorescence, center panels). Longitudinal optical sections through the protophloem (A) and xylem axis (B) planes are shown. Vascular cell types indicated by arrows in the magnified images (right panels) are color-coded with reference to the schematic overviews. (C-D) Simultaneous detection of PIN1 (anti-PIN1 antibody, red fluorescence) and PAX-CITRINE fusion protein (anti-GFP antibody, yellow fluorescence) by immunostaining, shown in longitudinal (C) and horizontal (D) view 3D reconstructions. (E) Examples of PIN1 'donut' and 'pancake' subcellular patterning in developing metaxylem vessels, detected by anti-PIN1 antibody staining. (F-G) Detection of PIN1 by anti-PIN1 antibody staining (red fluorescence) in developing metaxylem vessels, showing 3D reconstructions (left panels) and corresponding top-down views on the rootward end of individual vessels (right panels). (H-I) Quantification of the subcellular PIN1 pattern in developing metaxylem (MX) vessels in indicated genotypes. n=323-483 MX vessels; statistically significant differences (lower case letters) were determined by Fisher's exact test, p=0.0052.

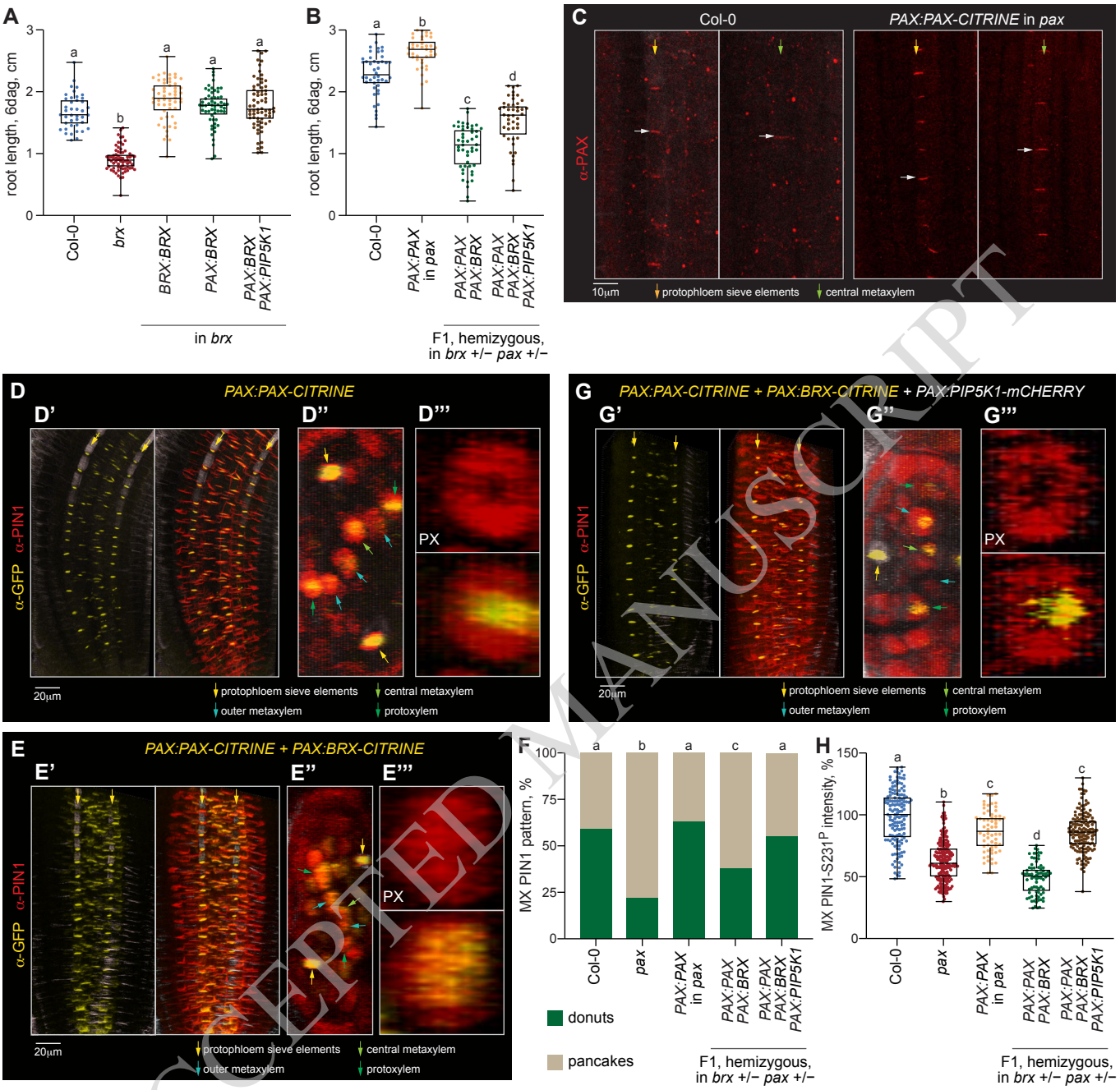

Figure 4. Ectopic expression of the PAX-BRX-PIP5K1 module in developing xylem vessels affects subcellular PIN1 patterning. (A-B) Primary root length of indicated genotypes. Transgenic PAX and BRX proteins were expressed as CITRINE fusions, PIP5K1 as an mCHERRY fusion. n=41-68 roots (A) and n=39-47 roots (B); statistically significant differences were determined by ordinary one-way ANOVA, $p<0.0001$ in (A) and (B). (C) Detection of native PAX in Col-0 wildtype or transgenic PAX-CITRINE fusion protein in *pax* mutant background by anti-PAX antibody staining (red fluorescence) in developing protophloem sieve elements (left panels) or metaxylem vessels (right panels). Note the higher expression level of transgenic fusion protein (e.g. white arrows) as compared to endogenous PAX. (D-E) Simultaneous detection of PIN1 (anti-PIN1 antibody, red fluorescence) and indicated CITRINE fusion proteins (anti-GFP antibody, yellow fluorescence) by immunostaining, shown in longitudinal (') and horizontal ('') overview, and top-down view in individual protoxylem (PX) vessels (''') (3D reconstructions). (F) Quantification of the subcellular PIN1 pattern in developing metaxylem (MX) vessels in indicated genotypes. n=142-182 MX vessels; statistically significant differences (lower case letters) were determined by Fisher's exact test, $p\leq0.0202$. (G) As in D-E. (H) Relative signal intensity of $S231^{P}$-specific PIN1 immunostaining in developing MX vessels of indicated genotypes. n=62-206 MX vessels; statistically significant differences (lower case letters) were determined by ordinary one-way ANOVA, $p\leq0.0007$. Box plots display 2nd and 3rd quartiles and the median, bars indicate maximum and minimum.

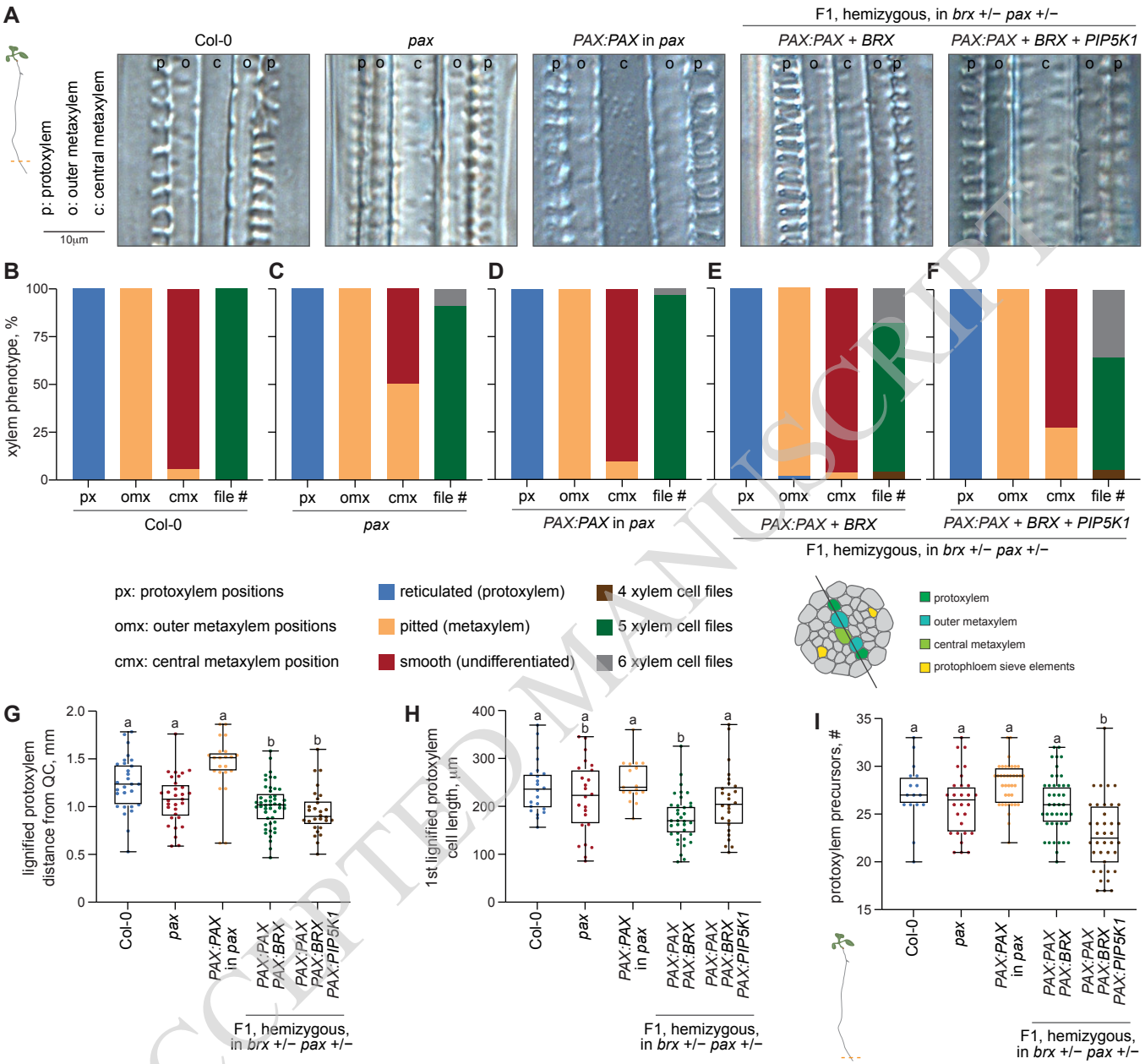

Figure 5. Ectopic assembly of the PAX-BRX-PIP5K1 module affects the trajectory of xylem development. (A-F) Differential interference contrast light microscopy example images of the xylem axis in the indicated genotypes, taken 5-7 mm above the root tip (A), and quantification of corresponding differentiation status per vessel type and genotype (B-F). n=22-35 roots. (G) Distance of the first lignified protoxylem vessels from the quiescent center (QC) in the indicated genotypes. n=22-48 roots; statistically significant differences (lower case letters) were determined by ordinary one-way ANOVA, $p \leq 0.0027$. (H) Length of the first lignified protoxylem (PX) vessels in the indicated genotypes. n=17-35 PX vessels; statistically significant differences (lower case letters) were determined by ordinary one-way ANOVA, $p \leq 0.0010$. (I) Number of undifferentiated vessel precursors in PX cell files until the first lignified PX vessel in the indicated genotypes, counted from the QC. n=16-43 cell files; statistically significant differences (lower case letters) were determined by ordinary one-way ANOVA, $p=0.0003$. Box plots display 2nd and 3rd quartiles and the median, bars indicate maximum and minimum.

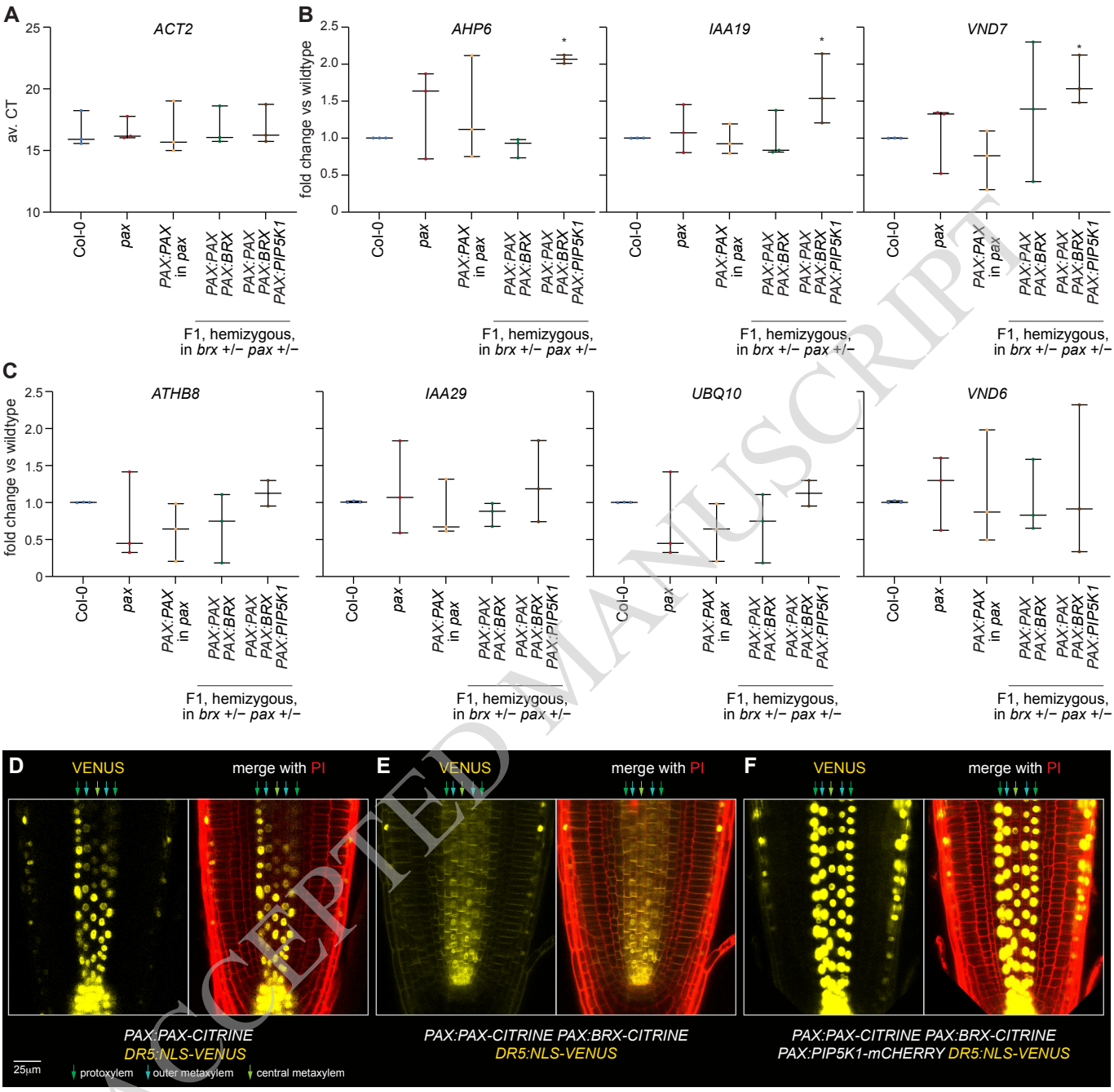

Figure 6. Ectopic PAX-BRX-PIP5K1 assembly affects xylem differentiation markers and auxin activity. (A-C) qPCR quantification of selected xylem development markers and control genes, normalized with respect to expression of the *ACTIN 2* (*ACT2*) housekeeping gene (A) and expressed as relative fold-change as compared to Col-0 wildtype (B-C). Plots display the averages of 3 technical replicates from 3 biological replicates each. Statistically significant differences (asterisks) were determined by Student's *t*-test compared to Col-0 wildtype, $p<0.001$ (*AHP6*), $p=0.042$ (*IAA19*), $p=0.008$ (*VND7*). (D-F) Confocal microscopy images of the auxin activity reporter *DR5:NLS-VENUS* in the presence of the indicated transgenes after crossing (all transgenes in hemizygous state). Yellow fluorescence: NLS-VENUS (nuclear signal) or PAX/BRX-CITRINE (plasma membrane signal); Red fluorescence: propidium iodide (PI) signal. Box plots display 2nd and 3rd quartiles and the median, bars indicate maximum and minimum.

Parsed Citations

Adamowski, M., and Friml, J. (2015). PIN-dependent auxin transport: action, regulation, and evolution. Plant Cell 27, 20-32.
Google Scholar: Author Only Title Only Author and Title

Adamowski, M., Narasimhan, M., Kania, U., Glanc, M., De Jaeger, G., and Friml, J. (2018). A Functional Study of AUXILIN-LIKE1 and 2, Two Putative Clathrin Uncoating Factors in Arabidopsis. Plant Cell 30, 700-716.
Google Scholar: Author Only Title Only Author and Title

Aliaga Fandino, A.C., and Hardtke, C.S. (2022). Auxin transport in developing protophloem: A case study in canalization. J Plant Physiol 269, 153594.
Google Scholar: Author Only Title Only Author and Title

Anne, P., and Hardtke, C.S. (2017). Phloem function and development-biophysics meets genetics. Curr Opin Plant Biol 43, 22-28.
Google Scholar: Author Only Title Only Author and Title

Barbosa, I.C., Zourelidou, M., Willige, B.C., Weller, B., and Schwechheimer, C. (2014). D6 PROTEIN KINASE activates auxin transport-dependent growth and PIN-FORMED phosphorylation at the plasma membrane. Dev Cell 29, 674-685.
Google Scholar: Author Only Title Only Author and Title

Barbosa, I.C., Shikata, H., Zourelidou, M., Heilmann, M., Heilmann, I., and Schwechheimer, C. (2016). Phospholipid composition and a polybasic motif determine D6 PROTEIN KINASE polar association with the plasma membrane and tropic responses. Development 143, 4687-4700.
Google Scholar: Author Only Title Only Author and Title

Barbosa, I.C.R., Hammes, U.Z., and Schwechheimer, C. (2018). Activation and Polarity Control of PIN-FORMED Auxin Transporters by Phosphorylation. Trends Plant Sci 23, 523-538.
Google Scholar: Author Only Title Only Author and Title

Bassukas, A.E.L., Xiao, Y., and Schwechheimer, C. (2022). Phosphorylation control of PIN auxin transporters. Curr Opin Plant Biol 65, 102146.
Google Scholar: Author Only Title Only Author and Title

Bishopp, A., Help, H., El-Showk, S., Weijers, D., Scheres, B., Friml, J., Benkova, E., Mahonen, A.P., and Helariutta, Y. (2011). A mutually inhibitory interaction between auxin and cytokinin specifies vascular pattern in roots. Curr Biol 21, 917-926.
Google Scholar: Author Only Title Only Author and Title

Blilou, I., Xu, J., Wildwater, M., Willemsen, V., Paponov, I., Friml, J., Heidstra, R., Aida, M., Palme, K., and Scheres, B. (2005). The PIN auxin efflux facilitator network controls growth and patterning in Arabidopsis roots. Nature 433, 39-44.
Google Scholar: Author Only Title Only Author and Title

Breda, A.S., Hazak, O., Schultz, P., Anne, P., Graeff, M., Simon, R., and Hardtke, C.S. (2019). A Cellular Insulator against CLE45 Peptide Signaling. Curr Biol 29, 2501-2508 e2503.
Google Scholar: Author Only Title Only Author and Title

Brunoud, G., Wells, D.M., Oliva, M., Larrieu, A., Mirabet, V., Burrow, A.H., Beeckman, T., Kepinski, S., Traas, J., Bennett, M.J., and Vernoux, T. (2012). A novel sensor to map auxin response and distribution at high spatio-temporal resolution. Nature 482, 103-106.
Google Scholar: Author Only Title Only Author and Title

Dettmer, J., Ursache, R., Campilho, A., Miyashima, S., Belevich, I., O'Regan, S., Mullendore, D.L., Yadav, S.R., Lanz, C., Beverina, L., Papagni, A., Schneeberger, K., Weigel, D., Stierhof, Y.D., Moritz, T., Knoblauch, M., Jokitalo, E., and Helariutta, Y. (2014). CHOLINE TRANSPORTER-LIKE1 is required for sieve plate development to mediate long-distance cell-to-cell communication. Nat Commun 5, 4276.
Google Scholar: Author Only Title Only Author and Title

Dhonukshe, P., Aniento, F., Hwang, I., Robinson, D.G., Mravec, J., Stierhof, Y.D., and Friml, J. (2007). Clathrin-mediated constitutive endocytosis of PIN auxin efflux carriers in Arabidopsis. Curr Biol 17, 520-527.
Google Scholar: Author Only Title Only Author and Title

Dhonukshe, P., Huang, F., Galvan-Ampudia, C.S., Mahonen, A.P., Kleine-Vehn, J., Xu, J., Quint, A., Prasad, K., Friml, J., Scheres, B., and Offringa, R. (2010). Plasma membrane-bound AGC3 kinases phosphorylate PIN auxin carriers at TPRXS(N/S) motifs to direct apical PIN recycling. Development 137, 3245-3255.
Google Scholar: Author Only Title Only Author and Title

Diaz-Ardila, H.N., Gujas, B., Wang, Q., Moret, B., and Hardtke, C.S. (2023). pH-dependent CLE peptide perception permits phloem differentiation in Arabidopsis roots. Curr Biol.
Google Scholar: Author Only Title Only Author and Title

Friml, J., Yang, X., Michniewicz, M., Weijers, D., Quint, A., Tietz, O., Benjamins, R., Ouwerkerk, P.B., Ljung, K., Sandberg, G.,

Hooykaas, P.J., Palme, K., and Offringa, R. (2004). A PINOID-dependent binary switch in apical-basal PIN polar targeting directs auxin efflux. Science 306, 862-865.
Google Scholar: Author Only Title Only Author and Title

Fujimoto, M., Arimura, S., Ueda, T., Takanashi, H., Hayashi, Y., Nakano, A., and Tsutsumi, N. (2010). Arabidopsis dynamin-related proteins DRP2B and DRP1A participate together in clathrin-coated vesicle formation during endocytosis. Proc Natl Acad Sci U S A 107, 6094-6099.
Google Scholar: Author Only Title Only Author and Title

Galvan-Ampudia, C.S., and Offringa, R. (2007). Plant evolution: AGC kinases tell the auxin tale. Trends Plant Sci 12, 541-547.
Google Scholar: Author Only Title Only Author and Title

Gerth, K., Lin, F., Daamen, F., Menzel, W., Heinrich, F., and Heilmann, M. (2017). Arabidopsis phosphatidylinositol 4-phosphate 5-kinase 2 contains a functional nuclear localization sequence and interacts with alpha-importins. Plant J 92, 862-878.
Google Scholar: Author Only Title Only Author and Title

Graeff, M., and Hardtke, C.S. (2021). Metaphloem development in the Arabidopsis root tip. Development 148.
Google Scholar: Author Only Title Only Author and Title

Grieneisen, V.A., Xu, J., Maree, A.F., Hogeweg, P., and Scheres, B. (2007). Auxin transport is sufficient to generate a maximum and gradient guiding root growth. Nature 449, 1008-1013.
Google Scholar: Author Only Title Only Author and Title

Heisler, M.G., Ohno, C., Das, P., Sieber, P., Reddy, G.V., Long, J.A., and Meyerowitz, E.M. (2005). Patterns of auxin transport and gene expression during primordium development revealed by live imaging of the Arabidopsis inflorescence meristem. Curr Biol 15, 1899-1911.
Google Scholar: Author Only Title Only Author and Title

Hirai, R., Higaki, T., Takenaka, Y., Sakamoto, Y., Hasegawa, J., Matsunaga, S., Demura, T., and Ohtani, M. (2019). The Progression of Xylem Vessel Cell Differentiation is Dependent on the Activity Level of VND7 in Arabidopsis thaliana. Plants (Basel) 9.
Google Scholar: Author Only Title Only Author and Title

Huang, F., Zago, M.K., Abas, L., van Marion, A., Galvan-Ampudia, C.S., and Offringa, R. (2010). Phosphorylation of conserved PIN motifs directs Arabidopsis PIN1 polarity and auxin transport. Plant Cell 22, 1129-1142.
Google Scholar: Author Only Title Only Author and Title

Ischebeck, T., Werner, S., Krishnamoorthy, P., Lerche, J., Meijon, M., Stenzel, I., Lofke, C., Wiessner, T., Im, Y.J., Perera, I.Y., Iven, T., Feussner, I., Busch, W., Boss, W.F., Teichmann, T., Hause, B., Persson, S., and Heilmann, I. (2013). Phosphatidylinositol 4,5-bisphosphate influences PIN polarization by controlling clathrin-mediated membrane trafficking in Arabidopsis. Plant Cell 25, 4894-4911.
Google Scholar: Author Only Title Only Author and Title

Kang, Y.H., and Hardtke, C.S. (2016). Arabidopsis MAKR5 is a positive effector of BAM3-dependent CLE45 signaling. EMBO Rep 17, 1145-1154.
Google Scholar: Author Only Title Only Author and Title

Kitakura, S., Vanneste, S., Robert, S., Lofke, C., Teichmann, T., Tanaka, H., and Friml, J. (2011). Clathrin mediates endocytosis and polar distribution of PIN auxin transporters in Arabidopsis. Plant Cell 23, 1920-1931.
Google Scholar: Author Only Title Only Author and Title

Kleine-Vehn, J., Huang, F., Naramoto, S., Zhang, J., Michniewicz, M., Offringa, R., and Friml, J. (2009). PIN auxin efflux carrier polarity is regulated by PINOID kinase-mediated recruitment into GNOM-independent trafficking in Arabidopsis. Plant Cell 21, 3839-3849.
Google Scholar: Author Only Title Only Author and Title

Kleine-Vehn, J., Wabnik, K., Martiniere, A., Langowski, L., Willig, K., Naramoto, S., Leitner, J., Tanaka, H., Jakobs, S., Robert, S., Luschnig, C., Govaerts, W., Hell, S.W., Runions, J., and Friml, J. (2011). Recycling, clustering, and endocytosis jointly maintain PIN auxin carrier polarity at the plasma membrane. Mol Syst Biol 7, 540.
Google Scholar: Author Only Title Only Author and Title

Koh, S.W.H., Marhava, P., Rana, S., Graf, A., Moret, B., Bassukas, A.E.L., Zourelidou, M., Kolb, M., Hammes, U.Z., Schwechheimer, C., and Hardtke, C.S. (2021). Mapping and engineering of auxin-induced plasma membrane dissociation in BRX family proteins. Plant Cell 33, 1945-1960.
Google Scholar: Author Only Title Only Author and Title

Kubo, M., Udagawa, M., Nishikubo, N., Horiguchi, G., Yamaguchi, M., Ito, J., Mimura, T., Fukuda, H., and Demura, T. (2005). Transcription switches for protoxylem and metaxylem vessel formation. Genes Dev 19, 1855-1860.
Google Scholar: Author Only Title Only Author and Title

Lavy, M., and Estelle, M. (2016). Mechanisms of auxin signaling. Development 143, 3226-3229.

Google Scholar: Author Only Title Only Author and Title

Mahonen, A.P., Bishopp, A., Higuchi, M., Nieminen, K.M., Kinoshita, K., Tormakangas, K., Ikeda, Y., Oka, A., Kakimoto, T., and Helariutta, Y. (2006). Cytokinin signaling and its inhibitor AHP6 regulate cell fate during vascular development. Science 311, 94-98.
Google Scholar: Author Only Title Only Author and Title

Mahonen, A.P., Ten Tusscher, K., Siligato, R., Smetana, O., Diaz-Trivino, S., Salojarvi, J., Wachsman, G., Prasad, K., Heidstra, R., and Scheres, B. (2014). PLETHORA gradient formation mechanism separates auxin responses. Nature 515, 125-129.
Google Scholar: Author Only Title Only Author and Title

Marhava, P., Bassukas, A.E.L., Zourelidou, M., Kolb, M., Moret, B., Fastner, A., Schulze, W.X., Cattaneo, P., Hammes, U.Z., Schwechheimer, C., and Hardtke, C.S. (2018). A molecular rheostat adjusts auxin flux to promote root protophloem differentiation. Nature 558, 297-300.
Google Scholar: Author Only Title Only Author and Title

Marhava, P., Aliaga Fandino, A.C., Koh, S.W.H., Jelinkova, A., Kolb, M., Janacek, D.P., Breda, A.S., Cattaneo, P., Hammes, U.Z., Petrasek, J., and Hardtke, C.S. (2020). Plasma Membrane Domain Patterning and Self-Reinforcing Polarity in Arabidopsis. Dev Cell 52, 223-235 e225.
Google Scholar: Author Only Title Only Author and Title

Moreira, S., Bishopp, A., Carvalho, H., and Campilho, A. (2013). AHP6 inhibits cytokinin signaling to regulate the orientation of pericycle cell division during lateral root initiation. PLoS One 8, e56370.
Google Scholar: Author Only Title Only Author and Title

Moret, B., Marhava, P., Aliaga Fandino, A.C., Hardtke, C.S., and Ten Tusscher, K.H.W. (2020). Local auxin competition explains fragmented differentiation patterns. Nat Commun 11, 2965.
Google Scholar: Author Only Title Only Author and Title

Morris, D.A., and Kadir, G.O. (1972). Pathways of auxin transport in the intact pea seedling (Pisum sativum L.). Planta 107, 171-182.
Google Scholar: Author Only Title Only Author and Title

Muto, H., Watahiki, M.K., Nakamoto, D., Kinjo, M., and Yamamoto, K.T. (2007). Specificity and similarity of functions of the Aux/IAA genes in auxin signaling of Arabidopsis revealed by promoter-exchange experiments among MSG2/IAA19, AXR2/IAA7, and SLR/IAA14. Plant Physiol 144, 187-196.
Google Scholar: Author Only Title Only Author and Title

Ramachandran, P., Augstein, F., Mazumdar, S., Nguyen, T.V., Minina, E.A., Melnyk, C.W., and Carlsbecker, A. (2021). Abscisic acid signaling activates distinct VND transcription factors to promote xylem differentiation in Arabidopsis. Curr Biol 31, 3153-3161 e3155.
Google Scholar: Author Only Title Only Author and Title

Rodrigues, A., Santiago, J., Rubio, S., Saez, A., Osmont, K.S., Gadea, J., Hardtke, C.S., and Rodriguez, P.L. (2009). The short-rooted phenotype of the brevis radix mutant partly reflects root abscisic acid hypersensitivity. Plant Physiol 149, 1917-1928.
Google Scholar: Author Only Title Only Author and Title

Rodriguez-Villalon, A., Gujas, B., Kang, Y.H., Breda, A.S., Cattaneo, P., Depuydt, S., and Hardtke, C.S. (2014). Molecular genetic framework for protophloem formation. Proc Natl Acad Sci U S A 111, 11551-11556.
Google Scholar: Author Only Title Only Author and Title

Sabatini, S., Beis, D., Wolkenfelt, H., Murfett, J., Guilfoyle, T., Malamy, J., Benfey, P., Leyser, O., Bechtold, N., Weisbeek, P., and Scheres, B. (1999). An auxin-dependent distal organizer of pattern and polarity in the Arabidopsis root. Cell 99, 463-472.
Google Scholar: Author Only Title Only Author and Title

Santuari, L., Scacchi, E., Rodriguez-Villalon, A., Salinas, P., Dohmann, E.M., Brunoud, G., Vernoux, T., Smith, R.S., and Hardtke, C.S. (2011). Positional information by differential endocytosis splits auxin response to drive Arabidopsis root meristem growth. Curr Biol 21, 1918-1923.
Google Scholar: Author Only Title Only Author and Title

Teale, W.D., Paponov, I.A., and Palme, K. (2006). Auxin in action: signalling, transport and the control of plant growth and development. Nat Rev Mol Cell Biol 7, 847-859.
Google Scholar: Author Only Title Only Author and Title

Tejos, R., Sauer, M., Vanneste, S., Palacios-Gomez, M., Li, H., Heilmann, M., van Wijk, R., Vermeer, J.E., Heilmann, I., Munnik, T., and Friml, J. (2014). Bipolar Plasma Membrane Distribution of Phosphoinositides and Their Requirement for Auxin-Mediated Cell Polarity and Patterning in Arabidopsis. Plant Cell 26, 2114-2128.
Google Scholar: Author Only Title Only Author and Title

Vaughan-Hirsch, J., Goodall, B., and Bishopp, A. (2018). North, East, South, West: mapping vascular tissues onto the Arabidopsis root. Curr Opin Plant Biol 41, 16-22.

Google Scholar: Author Only Title Only Author and Title

von der Mark, C., Cruz, T.M.D., Blanco-Tourinan, N., and Rodriguez-Villalon, A. (2022). Bipartite phosphoinositide-dependent modulation of auxin signaling during xylem differentiation in Arabidopsis thaliana roots. New Phytol 236, 1734-1747.
Google Scholar: Author Only Title Only Author and Title

Wang, Q., Aliaga Fandino, A.C., Graeff, M., DeFalco, T.A., Zipfel, C., and Hardtke, C.S. (2023). A phosphoinositide hub connects CLE peptide signaling and polar auxin efflux regulation. Nat Commun 14, 423.
Google Scholar: Author Only Title Only Author and Title

Watari, M., Kato, M., Blanc-Mathieu, R., Tsuge, T., Ogata, H., and Aoyama, T. (2022). Functional Differentiation among the Arabidopsis Phosphatidylinositol 4-Phosphate 5-Kinase Genes PIP5K1, PIP5K2 and PIP5K3. Plant Cell Physiol 63, 635-648.
Google Scholar: Author Only Title Only Author and Title

Weller, B., Zourelidou, M., Frank, L., Barbosa, I.C., Fastner, A., Richter, S., Jurgens, G., Hammes, U.Z., and Schwechheimer, C. (2017). Dynamic PIN-FORMED auxin efflux carrier phosphorylation at the plasma membrane controls auxin efflux-dependent growth. Proc Natl Acad Sci U S A 114, E887-E896.
Google Scholar: Author Only Title Only Author and Title

Willige, B.C., Ahlers, S., Zourelidou, M., Barbosa, I.C., Demarsy, E., Trevisan, M., Davis, P.A., Roelfsema, M.R., Hangarter, R., Fankhauser, C., and Schwechheimer, C. (2013). D6PK AGCVIII kinases are required for auxin transport and phototropic hypocotyl bending in Arabidopsis. Plant Cell 25, 1674-1688.
Google Scholar: Author Only Title Only Author and Title

Xiao, Y., and Offringa, R. (2020). PDK1 regulates auxin transport and Arabidopsis vascular development through AGC1 kinase PAX. Nat Plants 6, 544-555.
Google Scholar: Author Only Title Only Author and Title

Yamaguchi, M., Mitsuda, N., Ohtani, M., Ohme-Takagi, M., Kato, K., and Demura, T. (2011). VASCULAR-RELATED NAC-DOMAIN7 directly regulates the expression of a broad range of genes for xylem vessel formation. Plant J 66, 579-590.
Google Scholar: Author Only Title Only Author and Title

Zhao, Y. (2018). Essential Roles of Local Auxin Biosynthesis in Plant Development and in Adaptation to Environmental Changes. Annu Rev Plant Biol 69, 417-435.
Google Scholar: Author Only Title Only Author and Title

Zourelidou, M., Absmanner, B., Weller, B., Barbosa, I.C., Willige, B.C., Fastner, A., Streit, V., Port, S.A., Colcombet, J., de la Fuente van Bentem, S., Hirt, H., Kuster, B., Schulze, W.X., Hammes, U.Z., and Schwechheimer, C. (2014). Auxin efflux by PIN-FORMED proteins is activated by two different protein kinases, D6 PROTEIN KINASE and PINOID. Elife 3.
Google Scholar: Author Only Title Only Author and Title